An intercomparison campaign of ground-based UV-visible measurements of NO_2, BrO, and OClO slant columns: Methods of analysis and results for NO_2

A. C. Vandaele,[1] C. Fayt,[1] F. Hendrick,[1] C. Hermans,[1] F. Humbled,[1] M. Van Roozendael,[1] M. Gil,[2] M. Navarro,[2] O. Puentedura,[2] M. Yela,[2] G. Braathen,[3] K. Stebel,[4] K. Tørnkvist,[3] P. Johnston,[5] K. Kreher,[5] F. Goutail,[6] A. Mieville,[6] J.-P. Pommereau,[6] S. Khaikine,[7] A. Richter,[8] H. Oetjen,[8] F. Wittrock,[8] S. Bugarski,[9] U. Frieß,[9] K. Pfeilsticker,[9] R. Sinreich,[9] T. Wagner,[9] G. Corlett,[10] and R. Leigh[10]

Received 6 September 2004; revised 26 January 2005; accepted 23 February 2005; published 26 April 2005.

[1] Within the framework of the Network for the Detection of Stratospheric Change (NDSC), an intercomparison campaign of ground-based zenith-sky viewing UV-visible spectrometers was held at the Andøya Rocket Range (69°N, 16°E) at Andenes, Norway, from February 12 to March 8, 2003. The chosen site is classified as a complementary NDSC site. Eight groups from seven countries participated in the campaign which focused on the measurements of slant columns of NO_2, BrO, and OClO. This first campaign publication concentrates on measurements of the NO_2 slant columns. Different analysis criteria were investigated during the campaign. These included the use of fitting parameters as chosen by each group to provide what they considered to be optimized retrievals. Additional sets of parameters, imposed for all the groups, were also used, including the wavelength interval, absorption cross sections, and species fitted. Each instrument's results were compared to the measurements of selected reference instruments, whose choice was based on a technique combining regression analysis and examination of the residuals with solar zenith angle. Considering the data obtained during the whole campaign for solar zenith angles between 75° and 95°, all instruments agreed within 5% in the case of NO_2 with imposed analysis parameters in the 425–450 nm region. Measurements agree less well when retrieving the NO_2 slant columns in the 400–418 nm region or when using parameters optimized by each investigator for their instrument.

Citation: Vandaele, A. C., et al. (2005), An intercomparison campaign of ground-based UV-visible measurements of NO_2, BrO, and OClO slant columns: Methods of analysis and results for NO_2, *J. Geophys. Res.*, *110*, D08305, doi:10.1029/2004JD005423.

1. Introduction

[2] The Network for the Detection of Stratospheric Change (NDSC) was formed in 1986 and formally started in 1991, to provide a global ground based (GB) network making uniformly accurate measurements of stratospheric composition and structure for the earliest detection of stratospheric change, as well a long term reference for satellite observations of limited life time. Since its inception its role has been expanded to include tropospheric results where these are intrinsically available from the GB measurements. This extends the role of the NDSC to contribute to climate-change as well as ozone-climate related research issues. Another very important direction of the NDSC is the use of both archival data and special campaigns using NDSC instruments, to validate satellite measurements. The NDSC consists of five Primary Sites (Arctic, Northern Hemisphere Mid-Latitude, Equatorial, Southern Hemisphere Mid-latitude and Antarctic) together with many globally distributed Complementary Sites. These Complementary Sites host measurements identified as having specific benefit for the NDSC and include NDSC-class instruments operating at locations other than a NDSC Primary Station.

[3] The NDSC is structured in Working Groups, each covering a specific category of measurements. The inter-

[1]Belgian Institute for Space Aeronomy, Brussels, Belgium.
[2]Instituto Nacional de Tecnica Aerospacial, Torrejon de Ardoz, Spain.
[3]Norwegian Institute for Air Research, Kjeller, Norway.
[4]Polar Environmental Centre, Norwegian Institute for Air Research, Tromsø, Norway.
[5]National Institute of Water and Atmospheric Research, Omakau, Central Otago, New Zealand.
[6]Service d'Aéronomie du CNRS, Verrières le Buisson, France.
[7]Central Aerological Observatory, Dolgoprudny, Moscow Region, Russia.
[8]Institute of Environmental Physics, University of Bremen, Bremen, Germany.
[9]Institute of Environmental Physics, University of Heidelberg, Heidelberg, Germany.
[10]Space Research Centre, University of Leicester, Leicester, UK.

0148-0227/05/2004JD005423$09.00

comparison discussed in this paper was held under the umbrella of the NDSC UV-Visible Working Group. Further information is available on the NDSC web page: http://www.ndsc.ncep.noaa.gov/.

[4] Central to maintaining measurements of the highest uniformity and quality throughout the NDSC, is the use of instrument and analysis intercomparisons. Such campaigns are conducted by a formal referee, and are "blind" in that participants do not have access to the results of others, before submitting their own results. The first UV-Visible spectrometer intercomparison, for the measurements of stratospheric NO_2, was held in May 1992 at the NDSC southern hemisphere mid-latitude primary site at Lauder (45°S, 170°E) in New Zealand [*Hofmann et al.*, 1995]. It was attended by seven groups from seven countries and demonstrated that most groups could measure NO_2 column amounts at a solar zenith angle of 90° to within about ±10%, though the sensitivity of the individual instruments was found to vary considerably. Part of the variations was attributed to instrumentation, but also differences in the data analysis algorithms were identified. From these results, the following NDSC acceptance criteria for NO_2 measurements were accepted, based on scientific need: ability to measure a minimum $1 \pm 0.1 \times 10^{16}$ molec/cm^2 slant column at mid and low latitude stations and $2.0 \pm 0.8 \times 10^{15}$ molec/cm^2 in polar regions, and better than 5% (1σ) agreement with a reference instrument. Several groups were certified or partly certified following this campaign.

[5] A relevant, but not NDSC, NO_2 and O_3 comparison was held at Camborne (UK) in September 1994 between 11 European instruments in preparation for a common project (Second European Arctic and Mid-latitude experiment, SESAME) dedicated to the study of ozone destruction during winter in the Northern Hemisphere [*Vaughan et al.*, 1997]. The results showed that the SAOZ instruments to be deployed at several locations were consistent to within 3% (10 DU) for ozone and 5% for NO_2 though differences up to 10 % in ozone and 30 % in NO_2 could be found with other instruments. In some cases, these differences could be attributed to different absorption cross sections, but other sources of discrepancies were also evident. A prominent source of error identified was the uncertainty in the derivation of the amount of absorber in the reference spectrum.

[6] The second NDSC UV-Visible spectrometer intercomparison, for the measurement of stratospheric NO_2 and O_3 was held in June 1996 at the Observatoire de Haute Provence (44°N, 6°E) in France [*Roscoe et al.*, 1999]. It was attended by eleven groups from eight countries and demonstrated that significant improvements had been achieved since (and largely as a result of) the Lauder campaign. Slant columns were compared in two ways: by examining regression analyses against reference instruments over the whole range of zenith angles; and by taking fractional differences relative to a reference instrument at solar zenith angles between 85° and 91°. For O_3, regression slopes for the whole campaign agreed within 5% for most instruments, whereas similar agreement was only achieved for NO_2 when the same cross sections and wavelength intervals were used and only on a selected half-day's data. Mean fractional differences in NO_2 from a reference instrument were smaller than 7% (1σ) for most instruments, with standard deviations of 2%. The closest three instruments agreed to better than 2%. This campaign differed in the formality of intercomparison "blindness", in that in 1992 participants did not see the results of others until after the completion of the campaign and the submission of final results. This was deemed to be too restrictive because it limited the opportunity for participants to identify and correct major mistakes, such as might occur during instrument set-up. So, during the 1996 campaign all results were made available following the submissions of daily data by all groups, in plots that did not identify the individual groups. A similar protocol has been used in the present campaign.

[7] This, the third NDSC Intercomparison campaign of ground-based UV-visible instruments, was held at high latitude at the Andøya Rocket Range facility at Andenes (Norway, 69°N, 16°E), in the winter, from February 12 to March 8, 2003, when the NO_2 columns are expected to be minimum in the denoxified polar vortex. The Andøya Rocket Range is an NDSC complementary site. Eight groups participated. After a first week devoted to the installation of the instruments, the formal blind intercomparison of the instruments took place from February 21 to March 6, 2003. The referee was A.C. Vandaele, from the Université Libre de Bruxelles at the time of the campaign. Three molecules, NO_2, BrO, and OClO, were included in the exercise. The first aim of the intercomparison was to evaluate how well the NDSC selection criteria derived from the previous mid-latitude exercises could be met under polar conditions and to quantify the impact of possible improvements in instrumentation, algorithms and cross sections since the last campaign in 1996. The secondary objective was to assess the performance of halogen measuring instruments and to explore possible NDSC criteria for those species difficult to compare elsewhere. As a reminder, two types of acceptance criteria were adopted for NO_2, after the 1996 intercomparison [*Roscoe et al.*, 1999], which were characteristic of mid-latitude conditions: (1) Type I for global studies and trend measurements for which the instruments are asked to meet limits in the regression accuracy: Slope = 1 ± 0.05, Intercept = $\pm 0.15 \times 10^{16}$ molec/cm^2 and Residual $< 0.10 \times 10^{16}$ molec/cm^2 for NO_2, and Slope = 1 ± 0.03, Intercept = $\pm 0.15 \times 10^{19}$ molec/cm^2 and Residual $< 0.10 \times 10^{19}$ molec/cm^2 for O_3. (2) Type II for process studies and satellite validation for which the instruments are asked to reach the following criteria: Slope = 1 ± 0.10, standard deviation <0.05, offset = $\pm 0.25 \times 10^{16}$ molec/cm^2 for NO_2, and Slope = 1 ± 0.05, standard deviation <0.03 for O_3.

[8] This first publication describes the campaign organization, the instruments, and the results of the NO_2 intercomparison. Those relevant to BrO and OClO will be given in a further paper, although the general description of the measurement technique and the comparison tools developed in this paper are also valid for BrO and OClO.

2. Description of the Campaign

[9] The campaign took place at the research facility of the Andøya Rocket Range at Andenes in northern Norway. Daily measurements of meteorological data, such as temperature, pressure, wind speed and direction, as well as relative humidity, are performed routinely at the station. The

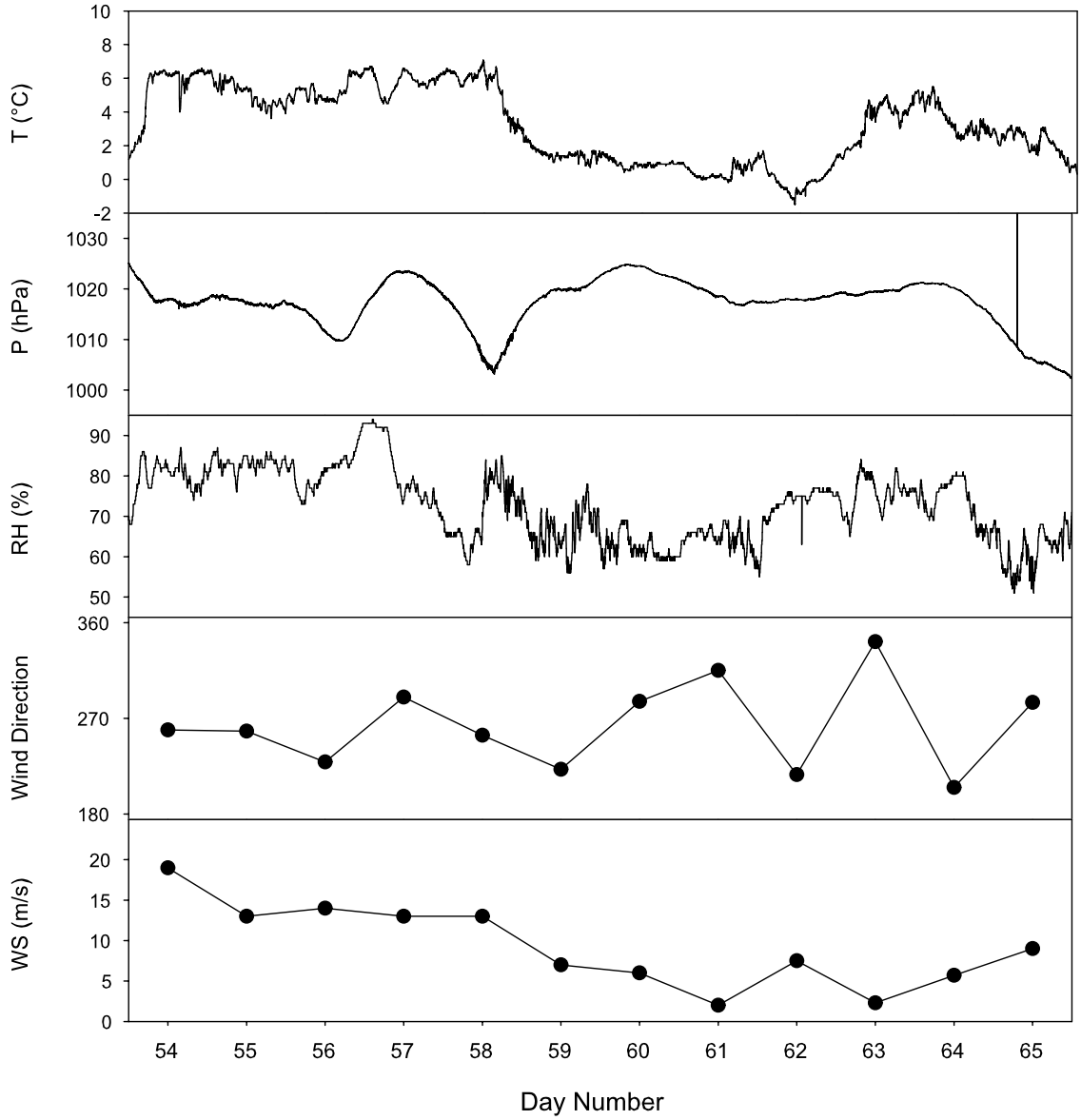

Figure 1. Evolution of the meteorological parameters during the NDSC campaign: Temperature, pressure, and relative humidity measured at 15 m elevation at the Andøya Rocket Range facility, and ECMWF wind speed and direction data (at 850 K).

facility also encompasses another measurement station, ALOMAR, Artic Lidar Observatory for Middle Atmosphere Research, located at the top of the 379 m high Ramman Mountain. The observatory is equipped with a Water Vapor radiometer, several irradiance sensors, a Brewer spectrophotometer and three Lidars (RMN, ozone and Na-Lidar). These provide information on polar stratospheric clouds, temperature, winds, OH and O_3 vertical profiles. In addition two UV-vis zenith sky viewing instruments, the SYMOCS 1 and 2 of NILU, are also present. Both participated in the intercomparison, as described in the following. In addition, two ozone sondes were launched on February17 and 26, and vertical profiles of temperature and ozone were obtained with the O_3-Lidar during February 20, 21, 26 and March 2.

[10] The campaign took place from February 12 to March 8, 2003. The first week was devoted to the installation and testing of the various instruments. The intercomparison exercise began February 21, when all instruments were sufficiently stabilized, and lasted until the March 6. The campaign was conducted as a blind exercise, however plots of measurements were shown and discussed daily by the groups without any indication of which data came from which group. No data were exchanged between the groups. Consolidated data were submitted within two months of the end of the campaign.

[11] Figure 1 illustrates the evolution of the meteorological parameters during the NDSC campaign. The conditions were rather exceptional for the location and time of year. This was the warmest February–March period of the last 44 years. Temperatures were rarely below zero during the campaign with no snowfall but substantial rainfall. The first part of the period, until day 58 (February 27) was very warm (6°C) for the season and particularly wet with fast wind (13–18 m/s) blowing from the W-SW. It was

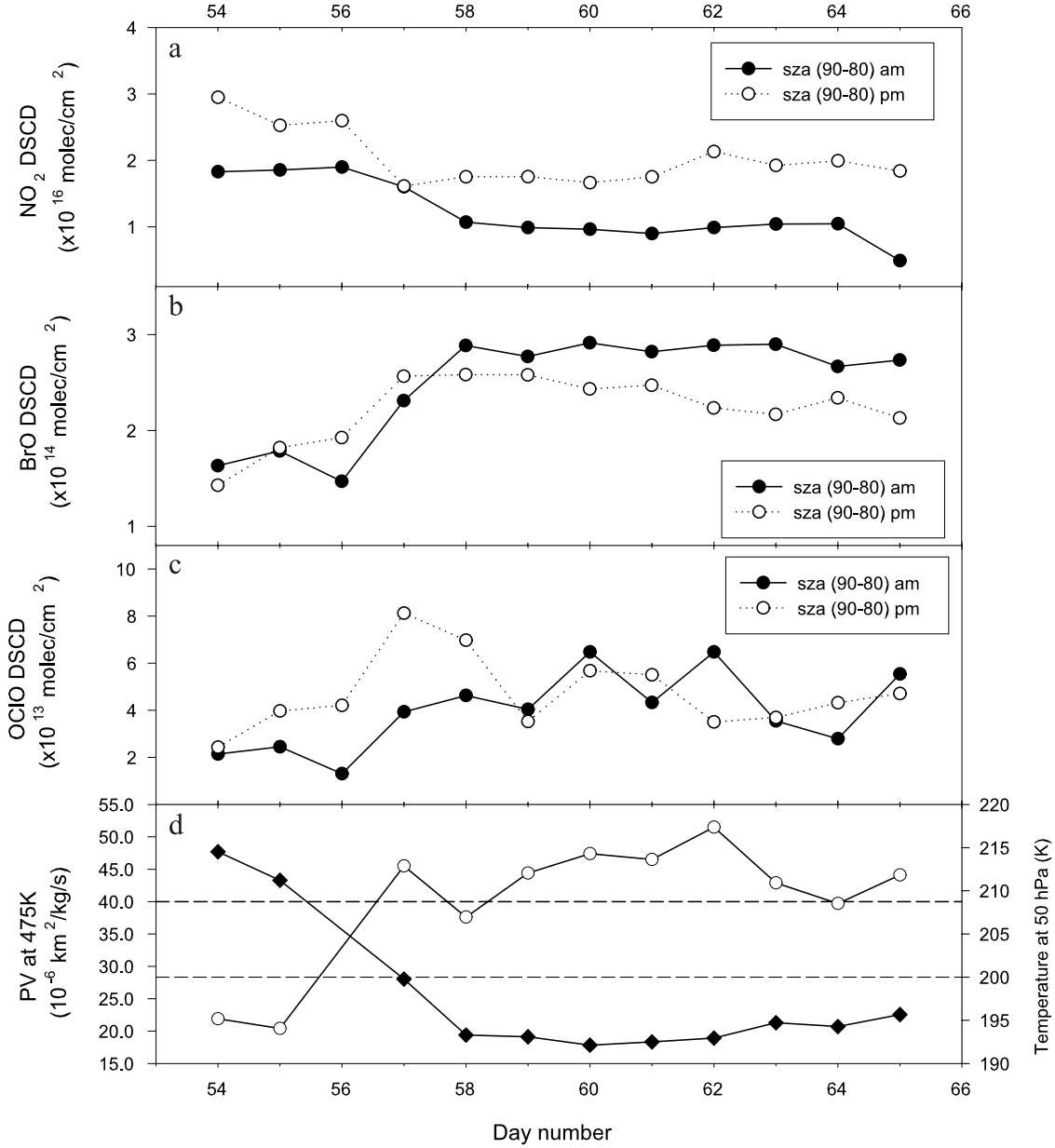

Figure 2. Evolution of the three target species during the campaign. (a) NO_2 DSCD at 90°–80° sza am and pm. (b) BrO DSCD at 90°–80° sza am and pm. (c) OClO DSCD at 90°–80° sza am and pm. (d) Potential vorticty (PV) at the 475 K isentropic level (open circles) and ECMWF temperature at 12 UT at 50 hPa (solid diamonds).

followed by four relatively cooler (0, +2°C) and dryer days in lighter and variable winds swinging from NW to SW, and terminated by a warmer weather.

[12] A schematic of the evolution of the three target species during the campaign is given in Figure 2, where differential slant column densities (DSCD) of NO_2, BrO and OClO at 90° solar zenith angle (sza), am and pm values, are reproduced. These values were obtained using a daily reference spectrum at 80° sza and are the reference values defined later in the text, which correspond to the average of the three best agreeing instruments. Potential vorticity at the 475 K level and temperature at 50 hPa are also plotted, indicative of the stratospheric conditions. In consistence with the warm stratospheric temperature and the low potential vorticity indicating that Andoya was located outside of the vortex, relatively large NO_2 columns could be observed during the first three days of the campaign, which dropped rapidly when the denoxified vortex moved over the station on February 26 (day 57) around noon, resulting in a fortuitous absence of diurnal variation on that day. Also in consistence with this picture, the very low BrO and OClO columns increased on that day, the first because of the diabatic descent of Br_y in the vortex, and the second, because of some chlorine activation. The magnitude of the BrO slant column at 90° sza in the vortex is similar to that reported in polar area during previous winters by *Tornkvist et al.* [2002]. In contrast, the $6-7 \times 10^{13}$ OClO molec/cm^2 are 3–4 times lower than the 2.5×10^{14} molec/cm^2 reported

by the same author at Ny-Ålesund during chlorine activated episodes. The vortex was only little activated in February 2003.

3. Instruments

[13] All 12 participating instruments were UV-visible zenith sky spectrometers whose acronyms are given in Table 1. Their main characteristics are also summarized in the table. The spectral range corresponds to the full range of the system and not the region actually used in the NO_2 retrieval procedure. The last columns indicate which molecules were detected by each of the instruments. Some groups used two instruments to cover all 3 requested species. Some of them were operated in MAX-DOAS mode [*Wittrock et al.*, 2004] and therefore spent less time measuring in the zenith-sky direction, which reduced the expected signal to noise ratio. The results of the horizon measurement mode was however not part of the intercomparison campaign.

[14] As light scattered at zenith is strongly polarized, the instruments must be insensitive to polarization. This can be achieved either by using bundles of optical fibers which mix up the polarization of the incoming light, or by recording always in the same plane of polarization. The latter method requires that the instrument tracks the sun continuously. All instruments, except IASB_2, CNRS, and NIWA_2 use fiber bundles to eliminate this problem. The IASB_2 instrument follows the solar azimuth at 90° and the CNRS and NIWA_2 instruments show small enough sensitivity to polarization not to affect the retrieval of the NO_2 slant columns.

[15] As requested by the NDSC protocol, instrumental functions were measured on site using a Hg lamp (Mercury, Krypton and Xenon pen ray lamp, operating in DC power supply, using in particular lines at 334, 346.6, 365, 435, 450, and 508 nm) and PTFE diffusers. Accurate knowledge of the instrumental spectral response function is essential for the convolution of the high-resolution laboratory cross sections of the measured species. It must be noted that some of the retrieval codes can also estimate this function and, more interestingly, its evolution with wavelength from the zenith sky spectra themselves [*Aliwell et al.*, 2002]. In order to evaluate the reliability of such a software facility, the measured slit functions were compared with functions deduced using the WINDOAS program, developed at Belgian Institute for Space Aeronomy (IASB/BIRA) [*Fayt and Van Roozendael*, 2001]. Results of the slit function comparison are plotted in Figure 3. For most of the instruments, the best agreement was found using a Gaussian type instrumental function. The IASB_1, NIWA_1, and NIWA_2 slit functions were however best reproduced using an error function. Due to its fixed entrance optics, the slit function of the CNRS instrument was not measured at Andøya. Those measurements were however performed at home just after the campaign and were thought to be representative of the instrument during the campaign. In general, the width of the instrumental function varies slightly on the recorded wavelength interval, as shown in Figure 4. Although in theory, the slit function of a grating spectrometer is a simple function of the deflection angle, larger dependences are usually found in actual instruments, due to improper optical design and/or alignment. The CNRS instrument shows the largest resolution variation, from 0.6 nm at the extremities of the detector to 1.5 nm at its middle point. In Figure 4 are also reported the limits of the TC1 and TC2 windows, as well as the TCO limits in the case of the CNRS and NILU instruments, both using larger spectral interval (see Table 2). Except for the CNRS instrument, the variation of the resolution for the TC1 and TC2, and therefore for most of the TC0 modes, is inexistent or very small. A larger variation of the resolution could be a problem for the retrieval of minor absorbers such as BrO and OClO. However, if regions of the spectra are used where changes are small, the effect should be small, if the right instrumental function is used for the convolution of the absorption cross sections. The IASB and NILU groups take into account the variation of the resolution across the detector, in their slant column retrieval. NIWA can also take this into account, but the instruments used in this campaign did not require this. In the case of the CNRS instrument, some tests were done with the WINDOAS program to retrieve the NO_2 slant column from the 410–530 nm spectral region, using either a NO_2 cross section convolved at the fixed resolution value of 1.5 nm (achieved in the TC1 window), or a NO_2 cross section convolved when taking into account the resolution variation. A typical difference of 0.7 % in slant columns was found compared to values derived by using a uniform 1.5 nm resolution.

[16] Another aspect, largely discussed in *Roscoe et al.* [1996], concerns the errors introduced when interpolating UV-visible spectra. The interpolation is needed because the retrieval technique, which will be detailed in section 4, requires the ratio of a pair of spectra, with possibly different wavelength calibrations. *Roscoe et al*. showed that in the case of the NO_2 retrieval, the instruments should have a resolution better than 1.0 nm, in order to avoid significant reduction of the NO_2 optical depth with a sampling ratio exceeding 4.5 pixel/FWHM. From Table 1, it can be seen that both conditions are verified for all instruments, except for CNRS, which has a resolution of about 1.5 nm in the TC1 window. However, in this region, the sampling ratio approaches the value of 5.

[17] The NDSC protocol also requires the measurements of stray light. A set of Schott filters (WG360, GG400, GG435, GG475, GG495, and OG550) was used to determine the magnitude of the stray light level for each instrument. This was obtained by taking the ratio of a zenith-sky spectrum to another one, close in time and filtered in the 350–370 nm region. Those instruments, for which this ratio was found to be smaller than 0.5 percent (0.005) were considered as having a good or very good stray light rejection capability. Other instruments, like the IASB_1, INTA, NILU_1, and NILU_2 exhibited larger stray-light levels (typically a factor of 10 higher), and could therefore be expected to show larger sensitivity to stray-light in their analysis. A more complete description of each instrument is given in the following sections.

3.1. CNRS Instrument

[18] The SAOZ instrument [*Pommereau and Goutail*, 1988] is based on a CP 200 Jobin Yvon spectrometer of 190 mm focal length with a 360 grooves/mm holographic grating allowing measurements on a spectral range of

Table 1. Characteristics of the Instruments of the 2003 NDSC Intercomparison Exercise

Group	Type	Grating, g/mm	Slit Width, μm	Field of View, °	Light Input System	Pol.	Detector	Spec Range, nm	Nb of Pixels	Res (FWHM, nm)	Samp Ratio (pixel/ FWHM)	MAX-DOAS	NO_2	BrO	OClO
							Service d'Aéronomie du CNRS								
CNRS	JobinYvon CP200	360	50	10	Quartz window	no	Hamamatsu PDA Ambient	300–620	1024	0.8–1.5	2.5–5		x	-	-
							Belgian Institute for Space Aeronomy								
IASB_1	Spectra PRO-150 Acton Res	1200	200	0.15° × 2°	Lens	no	Princeton NTE CCD 1340 400B −40°C	335–450	1340 × 400	0.75	9	x	x	x	x
IASB_2	TRIAX 180 Jobin Yvon	1800	200	0.15° × 2°	Lens	P	Hamamatsu −40°C	334–395	1024	0.7	11	x	-	x	x
							Instituto Nacional de Tecnica Aerospacial								
INTA	Jobin Yvon TRIAX 180	900	100	25	Fiber bundle	no	Princeton Inst PDA −40°C	325–460	1024	0.55–0.7	4–5		x	x	x
							Institute of Environmental Physics, Bremen								
IUPB_1	ARC 500 Acton Res	600	150	1	Fibre bundle	no	Princeton NTE CCD 1340 400B −40°C	324–408	1340 × 400	0.4	6	x	-	x	-
IUPB_2	Oriel MS260	600	100	1	Fibre bundle	no	Andor CCD DV 420-BU −38°C	336–504	1024 × 256	075–1.2	5–7	x	x	-	x
							Institute of Environmental Physics, Heidelberg								
IUPH	ARC 500 Acton Res	600	120	1	Fibre, lens	no	Hamamatsu PDA ST3904 −10°C	340–420	1024	0.55	7	x	x	x	x
							Norwegian Institute for Air Research								
NILU_1	SpectraPro 275(Acton Res)	1200	200	18	Fibre bundle	no	Spec 10: 100B CCD (Roper) −40°C	339–410	1034 × 100	0.45	9		-	x	x
NILU_2	SpectraPro 275(Acton Res)	600	150	18	Fibre Bundle	no	Reticon PDA Array −30°C	400–550	1024	1.2–1.4	8–9		x	-	-
							National Institute of Water and Atmosphere								
NIWA_1	ISA HR320	1200	200	14	Fibre	no	Hamamatsu CCD −20°C	330–390	1024 × 128	0.55	11		-	x	x
NIWA_2	SPEX 270M	964	250	5	Mirror	no	Hamamatsu CCD −20°C	400–490	1024 × 128	0.66	8		x	-	-
							Space Research Centre, Leicester								
ULEI	Oriel MS257i	Varied during the campaign			Fibre, lens	no	Marconi 47–20 CCD −42.5°C	395–480	1072 × 1033	0.8–1.0	9	x	x	-	-

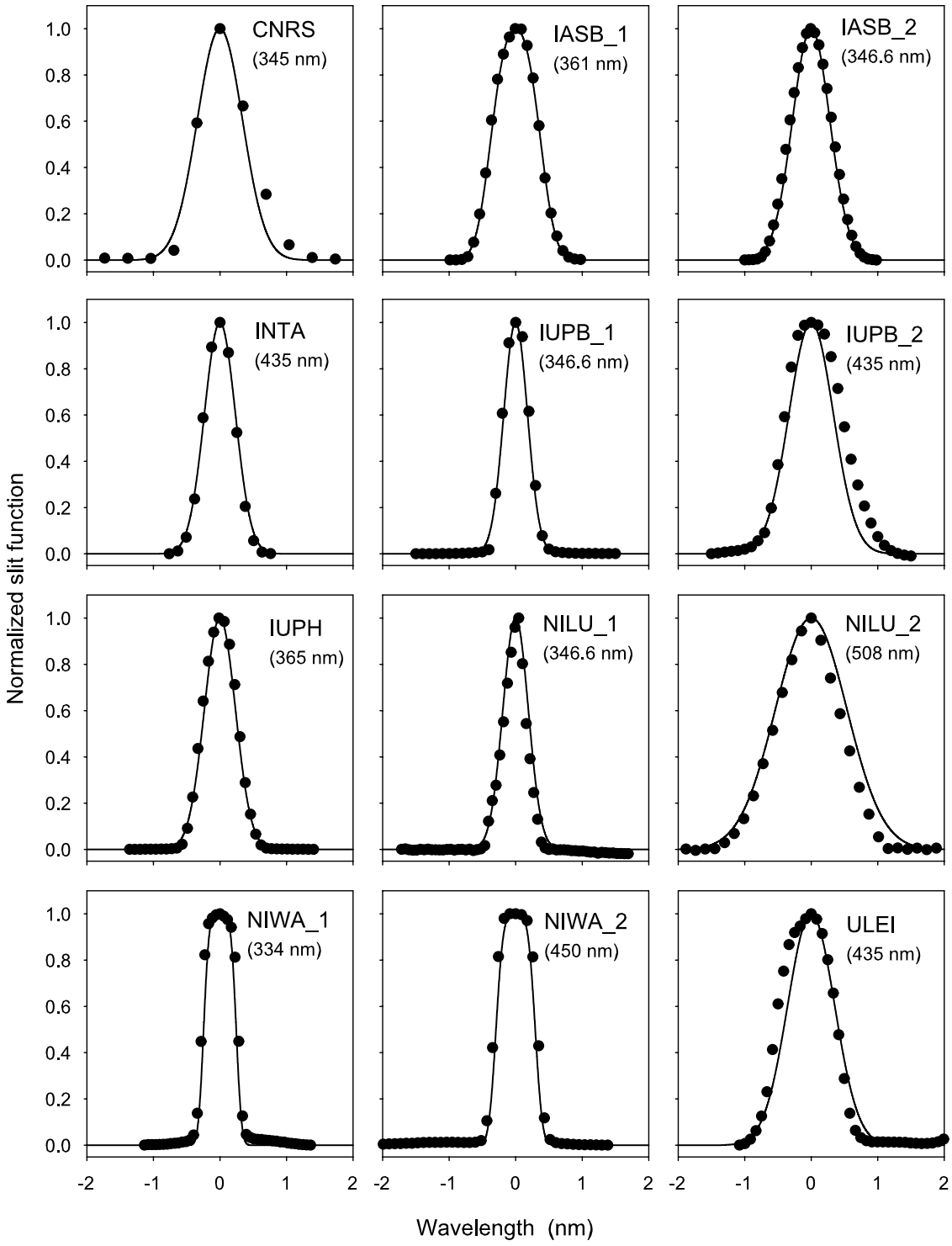

Figure 3. Slit functions of all participating instruments. Measured functions using a Hg lamp are represented by dots, while solid lines show the functions derived from zenith sky spectra using the WINDOAS program.

320 nm, typically from 300 to 620 nm, with a 1.1 nm resolution. The detector is a linear array 1024 PDA from Hamamatsu, thus allowing a sampling ratio of 2.9, working at room temperature providing a 14 bits dynamic range. The instrument is designed for the monitoring of ozone and NO_2 over a broad spectral range of respectively 451–619 nm and 410–530 nm for using a maximum number of absorption bands and thus removing at best interferences. This arrangement is not suitable for measuring BrO or OClO or reducing the spectral range of the NO_2 measurements, e.g. 425–450 nm or 400–418 nm as requested during the comparison exercise. The equipment is installed into an insulated box,

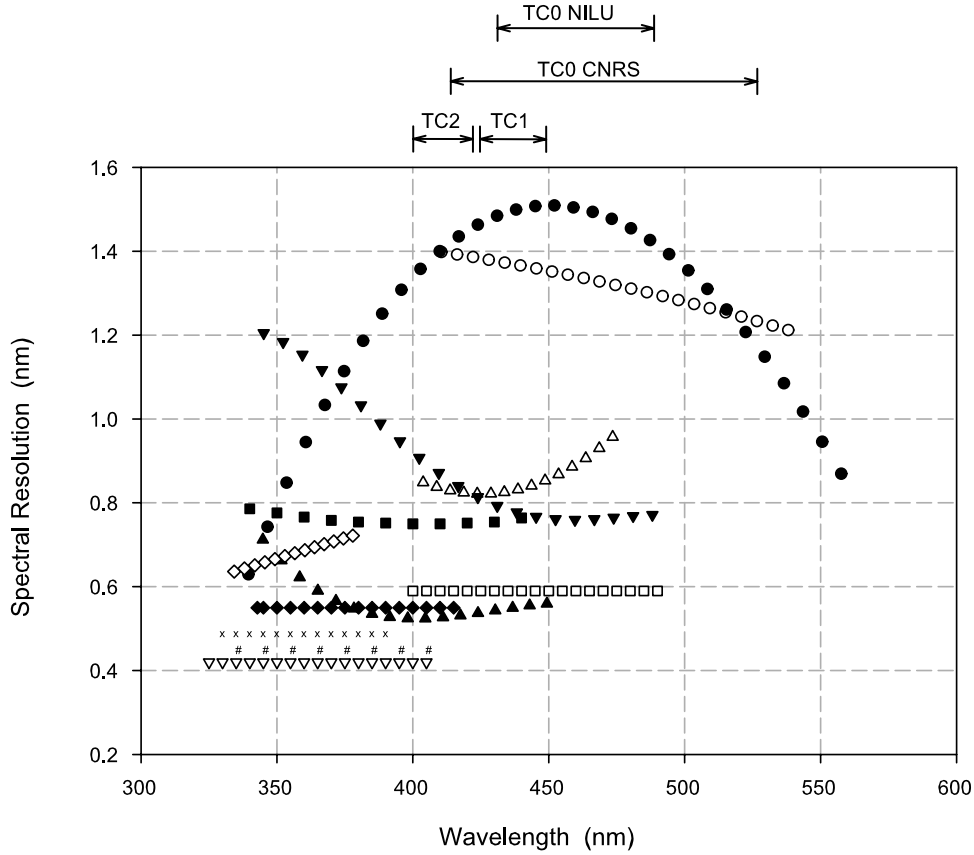

Figure 4. Wavelength dependence of instrument functions determined by WINDOAS from zenith sky spectra. The spectral interval is restricted compared to the full range of the instrument because of edge effects in the calculation (solid circles, CNRS; solid squares, IASB_1; open diamonds, IASB_2; solid triangles, INTA; open inverted triangles, IUPB_1; solid inverted triangles, IUPB_2; solid diamonds, IUPH; number signs, NILU_1; open circles, NILU_2; crosses, NIWA_1; open squares, NIWA_2; open triangles, ULEI).

while the light is collected through a quartz window. The field of view delimited by a baffle system is ±10° in respect to zenith. The time is set by a GPS system. Instrument activation, exposure duration (from 0.7 to 52 s), dark current and measurement cycles, as well as spectral and ancillary data extraction are controlled by a central CPU. The measurements are repeated every 60 s. The spectral analysis is performed by a homemade SAM software. The post-campaign reprocessing of the data has shown that the spectral characteristics of the instrument were not optimum during the campaign (resolution of 1.5 nm instead of 1.1 nm at 450 nm, and wavelength dependence of the resolution) compared to usual adjustments. The reprocessing accounts for this degradation.

3.2. IASB/BIRA Instrument

[19] IASB/BIRA operated two spectrometers, IASB_1 and IASB_2. Both instruments are designed to collect scattered light at zenith and in three additional directions close to the horizon (3°, 7.5° and 12.5°). Zenith and off-axis viewing directions are successively scanned with a total repeating rate of approximately 8 min. In case of IASB_1, the multi-axis viewing geometry is achieved by a moving telescope (50 mm focal length) attached to a quartz fiber optic that transmits the light to the spectrometer. The field of view is less than 1 degree full angle. For IASB_2, the multi-axis scanning is obtained by a moving mirror placed in front of the entrance slit of the spectrometer. With a lens of 50 mm, the field of view is reduced to 0.2° × 2.8° full angle.

[20] The IASB_1 spectrometer is a SpectraPro-150 from Acton Research mounted with a grating of 1200 grooves/mm so that the spectral range from 335 to 450 nm is covered with a spectral resolution of approximately 0.75 nm FWHM. The detector used is a backside illuminated CCD of the Princeton NTE/CCD-1340/400B type supplied by Roper Scientific and operated at the temperature of −40°C. The chip size is 1340 × 400 pixels. Tracks are binned vertically by software. The second spectrometer (IASB_2) is a TRIAX-180 from Jobin-Yvon equipped with a grating of 1800 grooves/mm. It covers the spectral range from 334 to 395 nm with a spectral resolution of 0.7 nm FWHM and a sampling ratio of 11 pixels/FWHM. The spectrometer is linearly polarized and mounted vertically on a rotating plate that follows the solar azimuth. The detector is a linear diode array from Hamamatsu supplied with the acquisition electronics by Princeton Instruments and cooled to the temperature of −40° C. Both instruments are insulated and thermally stabilized to better than 1°K.

[21] The data acquisition is fully automated using software developed at IASB/BIRA. The spectral analysis is

Table 2. Description of the TC0 Settings of All Instruments for NO_2[a]

CNRS 410–530			IASB 425–450 (TC1)			INTA 425–450 (TC1)		
O_3	Bd 223	-	O_3	Bd 223, 243	(1×10^{20})	O_3	Bd 223, 243	(1×10^{20})
NO_2	V 220	(1×10^{16})	NO_2	V 220	(2.5×10^{16})	NO_2	V 220	(5×10^{16})
O_4	Gr mod		O_4	Gr		O_4	Gr	
H_2O	Hi		H_2O	Hi		H_2O	Hi	
Ring	From Ref spectrum		Ring	Vrz		Ring	Vrz	
Offset	-		Offset	Deg 1		Offset	1/ref	
Poly	-		Poly	3		Poly	3	

IUPB 425–450			IUPH 400–418 (TC2)			NILU 434–480		
O_3	Bd 223	-	NO_2	V 220	(2.5×10^{16})	O_3	B 221	
NO_2	V 220	(1×10^{16})	OClO	K 213		NO_2	Ha 227	
O_4	Gr					O_4	H	
H_2O	BR					H_2O	Hi	
Ring	Bremen		Ring	Vrz		Ring	Vrz	
Offset	cst		Offset	cst		Offset	cst	
Poly	2		Poly	2		Poly	3	

NIWA 425–452.5			ULEI 425–450 (TC1)		
O_3	Bd 223	(1×10^{20})	O_3	Bd 223,243	(1×10^{20})
NO_2	V 220	(1×10^{16})	NO_2	V 220	(2.5×10^{16})
O_4	H		O_4	Gr	
H_2O	Har		H_2O	Hi	
Ring	Vrz + slope		Ring	Vrz	
Offset	cst		Offset	cst	
Poly	2, 3		Poly	3	

[a]Letters refer to the following literature cross sections: B, *Burrows et al.* [1998]; Bd, Bogumil deconvoluted [*Bogumil et al.*, 2000]; BR, *Coheur et al.* [2002]; Gr, *Greenblatt et al.* [1990] corrected for shift and stretch; H, *Hermans et al.* [2002]; Ha, *Harder et al.* [1997]; Har, *Harder and Brault* [1997]; Hi, Hitran 2000 [*Rothman et al.*, 2003]; K, *Kromminga et al.* [2003]; V, *Vandaele et al.* [1998]; Vrz, Ring calculated with WINDOAS [*Fayt and Van Roozendael*, 2001]. Numbers after these acronyms indicate the temperature at which the cross sections were obtained. Numbers in parentheses are the Io correction factors (see text).

performed using the WINDOAS software also developed at IASB/BIRA.

[22] IASB_1 was operated nominally during the whole campaign duration, while IASB_2 suffered from two successive problems that altered the time coverage and the reliability of the measurements. First, one of the spectrometer's mirrors (the focusing mirror) was damaged during the transport to Andøya and had to be replaced on-site, which resulted in a loss of spectral resolution due to imperfect optical alignment. Second, the diode array detector encountered thermal shock during its first cooling process, which first resulted in added noise in the measured spectra and finally definitive breakdown of the instrument on February 26.

3.3. INTA Instrument

[23] The instrument of the INTA group is designed to allow the measurement of BrO, NO_2 and OClO with the same detector. It is based on a Jobin Yvon TRIAX 180 spectrograph of 180 mm focal length with a 900 grooves/mm grating which provides a spectral range of 135 nm. The grating is orientated to cover the 325–460 nm spectral range and is blazed at 300 nm to produce a uniform grating efficiency over this spectral band. The detector is an evacuated 1024 PDA controlled by a ST-125 from Princeton Instruments providing 16 bits dynamical range, cooled to −40°C with the assistance of a circulating cryostat.

[24] Light is collected by mean of a depolarizing 5-metre quartz fiber bundle of 0.9 mm in diameter and a numerical aperture of 0.22. The rectangular end of the bundle of 6 mm × 100 microns, acting as entrance slit. The spectrograph housing is insulated and regulated to keep the instrument thermally stabilized to within 0.1 K.

[25] The overall control of the instrument, scheduling, twilight routines, GPS time and spectral and ancillary data extraction is performed by a homemade software. Spectra at 90% of the saturation level are accumulated for the time required for the sun to cover 0.2° sza providing 5 spectra per degree except at very large solar zenith angles when not enough light is available. To extend the measurements to larger sza, the 0.2° criterion is rescheduled to larger values according to a twilight function that accounts for the rapid change of illumination.

3.4. IUPB Instrument

[26] The instruments of the Bremen group are able to collect light that is scattered not only at zenith but also in directions close to the horizon. Here, successively three off-axis directions (3°, 7.5° and 12.5°) and the zenith are scanned with a temporal resolution of five minutes overall whereof two minutes are spent for the zenith. This multi-axis viewing geometry is achieved by a moving mirror in the telescope. The light is transmitted to two spectrographs using a split quartz fiber bundle. With this MAX-DOAS technique, vertical profile information for atmospheric absorber can be derived [*Wittrock et al.*, 2004]. However some time is lost for the zenith-sky measurements discussed in this paper, which will inevitably have an effect on the signal to noise ratio.

[27] The two spectrographs together cover a wavelength region from 324 to 504 nm. The ARC 500 from Acton Research has a focal length of 500 mm and is operated with

a grating with 600 grooves/mm. The detector used for this spectrograph is a CCD (Charge-Coupled Device) of Princeton NTE/CCD-1340/400-EMB type supplied by Roper Scientific. The chip has a size of 1340 × 400 pixels, is cooled to −40°C and operated in full vertical software binning. In the wavelength region from 324 to 408 nm a spectral resolution of about 0.4 nm is obtained. Here, this set up is referred to as IUPB_1. As second spectrograph the Oriel MS 260 also with a grating of 600 grooves/mm is used. The focal length of this instrument is 260 mm. The wavelength region was chosen to be from 336 to 504 nm. The CCD is a DV 420-BU provided by Andor Technology and is cooled to −38 °C. The chip is composed of 1024 × 256 pixels. This set-up yields a spectral resolution of 0.75 to 1.2 nm depending on the wavelength and is abbreviated as IUPB_2. Both spectrographs are insulated and thermally stabilized to within 0.1 K.

[28] The synchronization of the two spectrographs as well as the detectors with the telescope is operated by software written in Bremen. Automated calibration measurements including dark current, white light and line lamp measurements were carried out daily at night. Also the slant column retrieval was performed using Bremen's own software.

[29] For both instruments, difficulties were encountered during the campaign: The detectors suffered from a memory effect that led to the contamination of the measurements after changes in intensity or light source such as after calibration. In addition, measurements of the visible instrument, IUPB_2 were sometimes distorted by a periodic noise signal of several counts amplitude that correlated with NO_2 absorption structures. Both effects, which could not be reproduced in the laboratory in Bremen after the campaign, could not be fully corrected in the spectra and therefore had a negative impact on quality of the slant columns.

3.5. IUPH Instrument

[30] The IUPH performed zenith- sky observations of scattered sunlight using an ARC 500 spectrograph from Acton Research with a focal length of 500 mm. The light is collected using a small telescope, consisting of a quartz glass lens and a color glass filter (UG5) that reduces the instrumental stray light. The lens focuses the incoming light on the entrance of a depolarizing fiber bundle consisting of 14 individual quartz fibers of 120μm diameter. At the other end of the bundle, the fibers are arranged as a column, serving as the entrance slit for the spectrograph.

[31] The light is dispersed using a grating with 600 grooves/mm, covering a wavelength range between 340 and 420 nm, and detected using a photo diode array (Hamamatsu ST3904). The photo diode array consists of 1024 individual Si CMOS photo diodes of 2.5mm height and 25μm width. The detector is cooled to (−10 ± 0.1)°C using a two-stage thermoelectric Peltier cascade. The whole spectrograph unit is located inside an insulated box and kept at a constant temperature of (30 ± 0.1)°C in order to avoid any changes in the adjustment of the instrument.

[32] The measurement is controlled by a homemade software. Zenith-sky spectra are acquired each 3 minutes for solar zenith angles smaller than 88°. The integration time is increased at larger solar zenith angles to achieve a better signal-to-noise ratio during twilight. Reference spectra of offset and dark current are automatically recorded each night.

[33] Unfortunately, mechanical problems with the entrance telescope occurred during the campaign. The telescope had to be removed, and the operation of the instrument without a lens in front of the entrance of the fiber bundle lead to an increase in the field of view from less than 1° to approximately 15°. However, the air mass factors for stratospheric absorbers do not change significantly between zenith direction and a viewing angle of 15°. We therefore expect our results to be unaffected by the removal of the telescope.

3.6. NILU Instrument

[34] NILU has developed and deployed two zenith-sky viewing spectrometer systems, SYMOCS (SYstem for MOnitoring Compounds in the Stratosphere)-VIS and SYMOCS-UV, for observation of stratospheric O_3, NO_2, OClO and BrO from the ground (for a description of the instruments, see *Tornkvist* [2000]). Since summer 1998 the instruments are located at the Andøya Rocket Range. Scattered light from the zenith sky is collected by optical quartz fiber bundles, which depolarize the incoming light. The field of view is 18° (full angle). Both spectrometer systems consist of a f/3.2 Czerny-Turner spectrograph (Acton Research Corporation) with a focal length of 275 mm. The wavelength range covered by the two instruments is 339–410 nm (SYMOCS-UV) and 400–550 nm (SYMOCS-Vis). The SYMOCS-UV has an entrance slit width of 200 μm and a grating of 1200 grooves/mm, which results in a spectral resolution of 0.45 nm and an over sampling of 9 pixel/FWHM. The entrance slit width of the SYMOCS-VIS is set to 150 μm. This, together with a focal length of 0.275 m and the grating of 600 grooves/mm, gives a spectral resolution of approximately 1.0 nm and a sampling ratio of approximately 9.

3.7. NIWA Instrument

[35] NIWA used two instruments that were built for the Andøya campaign and subsequently deployed for measurements at Lauder. NIWA_1 is an ISA-HR320 Czerny Turner Flat-Field F/5 spectrometer with a 1200 g/mm plane holographic grating from Richardson Grating Laboratory (RGL). The detector is a Hamamatsu C7042 Multichannel Detector Head with a back-thinned CCD, 1024 × 128 × 24 micron pixels, operating in line-binning mode (FFT) and cooled to −20°C. The wavelength range covered is 330–390 nm resulting in a sampling ratio of 11 pixels per resolution element (0.55 nm). A 0.75 m fiber optic is used to feed the light from a 100 mm quartz lens into the entrance slit providing scrambling of sky polarization and a narrow field of view (1°). Unpolarized operation was chosen for the campaign to match the majority of instruments used, although a polarizer was subsequently added for use at Lauder. This is preferred because it reduces the spectral fitting errors due to Ring effect.

[36] NIWA_2 is a SPEX-270M F/4 imaging spectrometer with an RGL 964 g/mm plane ruled grating. The detector head is the same model Hamamatsu C7042 head, as used for NIWA_1. The wavelength range is 400 to 490 nm resulting in a sampling ratio of 8 pixels per resolution element (0.66 nm). The entrance slit views the sky directly

Table 3. Definition of TC1 and TC2 Test Cases[a]

Test Case	Wavelength Interval, nm	Abs. Cross Sections
TC1	425–450	O_3 (Bd 223K), NO_2 (V 220K), O_4 (Gr), H_2O (Hi)
TC2	400–418	NO_2 (V 220K), OClO (K 213K)

[a]See Table 2 for the definition of the acronyms.

via a baffled 45° mirror so the grating polarization characteristics determine spectrometer polarization. With the ruled grating the difference in transmission (<20%) between the two axes is less than the NDSC maximum specification (see NDSC Instrument Specific Appendix on NDSC Web page hhtp://www.ndsc.ncep.noaa.gov). Both NIWA spectrometers were modified to reduce stray light by adding extra baffling to reduce scattered zero order light and to block the detector's view of the collimating mirror.

3.8. ULEI Instrument

[37] The University of Leicester's Multi-Axis DOAS instrument is based on the concept of imaging spectra from multiple fixed telescopes concurrently on to a single CCD through the use of a multi-track fiber and an imaging spectrometer. The hardware system is capable of handling up to 5 axes simultaneously, however during the campaign only two axes were recorded with data submitted from zenith measurements only.

[38] The head-unit consists of five fixed telescopes with 5cm diameter pointing at 0° (Zenith), 75°, 80°, 85° and 90°. Scattered solar radiation is focused by these telescopes into 10-metre 200 μm-diameter fiber-optic cables connected to a 9-track fiber-optic alignment system, which places the output of all fibers in vertical alignment at the entrance slit of an Oriel MS257 imaging spectrometer. All fibers are imaged simultaneously onto a Marconi 47–20 back-illuminated frame-transfer CCD with 1072 columns and 1033 rows. Each fiber image covers approximately 30 rows of the CCD with 100 rows separation between images. Sections of CCD between imaged fibers are recorded and analyzed to monitor for stray light, dark current and information transfer between spectral images. During the campaign stray light and information transfer were found to be negligible, with dark current signal structure exhibiting only broadband and stable structure which was subtracted in software with any residual structure being removed by the mechanics of the DOAS technique. During the campaign spectral extraction was performed by software written at the University of Leicester, with the DOAS retrieval performed by the WinDOAS package written at the Belgian Institute for Space Aeronomy, Brussels.

[39] This instrument, with its concurrent imaging capability has potential for multi-axis measurements at high temporal resolution. However, during this campaign the instrument was in an early stage of development and therefore was operating in a basic dual-axis mode at low temporal resolution.

4. Measurement Technique

[40] The measurement technique will only be briefly summarized here. Extended discussion of the method can be found, e.g., in *Platt* [1994] and *Lee et al.* [1994]. The determination of the slant columns of the target species is based on the DOAS technique (Differential Optical Absorption Spectroscopy), applied on a zenith-sky spectrum $I(\lambda)$ ratioed to a reference solar spectrum, obtained at high sun, $I_{ref}(\lambda)$. Differential slant column densities (DSCD) are derived by least squares fitting using the following equation:

$$\ln\left(\frac{I(\lambda) - offset(\lambda)}{I_{ref}(\lambda)}\right) = -\sum_i \sigma_i(\lambda) DSCD_i - P(\lambda) \quad (1)$$

here $\sigma_i(\lambda)$ is the differential absorption cross-sections of species i, $P(\lambda)$ is a polynomial function representative of the Rayleigh and Mie scattering. The $offset(\lambda)$ parameter is necessary to account for possible instrumental or atmospheric stray light or residual dark current signal. The apparent linearity of equation (1) is impaired by the existence of shifts and stretches of the wavelength, which are required to best align the $I(\lambda)$ spectrum and the absorption cross-sections on $I_{ref}(\lambda)$. Fraunhofer lines present in the spectra are used by most of the participating groups to calibrate the wavelength scale. The standard procedure for wavelength calibration commonly in used within NDSC is to fit zenith-sky spectra to a highly accurate reference solar spectrum [*Kurucz et al.*, 1984] after proper convolution and scaling. The resulting wavelength grid assignment can be made accurate to better than 0.01 nm depending on instrumental performance [see, e.g., *Aliwell et al.*, 2002].

[41] When trying to compare several instruments in order to assess the reasons for the observed differences, parameters used in the retrieval procedures should be similar. Three different test cases (TCs) were defined for each molecule, and corresponded to sets of well-defined analysis parameters, including the wavelength interval, the choice of cross sections, and the species fitted. TC0 was chosen as being the open choice of parameters according to what each group considered to be its optimized retrievals. Table 2 indicates the different parameters' values used by each group for NO_2. The definitions of TC1 and TC2 are indicated in Table 3. TC1 set of parameters corresponds to the widely used 425–450 nm spectral interval, whereas TC2 set extracts the NO_2 column at UV wavelengths (400–418 nm). This region has been recommended by *Preston et al.* [1997] as being more suitable for NO_2 profile retrieval.

[42] Supplementary parameters needed for the analysis are the polynomial degree of $P(\lambda)$ and the pseudo cross section accounting for the so-called Ring effect, which were also dictated in the TC1 and TC2 settings. The polynomial order was chosen to be 2. The Ring effect has its origin in inelastic scattering processes, mainly the rotational Raman scattering by molecular O_2 and N_2, taking place in the atmosphere. It results in a broadening of the solar and atmospheric features present in the observed spectra. This

broadening has a large impact on minor absorbers such as BrO or OClO, whose structures may be completely masked by the Ring features. Ring cross sections can be determined using different methods. The chosen Ring cross section was obtained with the help of the WINDOAS program [*Fayt and Van Roozendael*, 2001]. It was, however, decided not to impose the offset parameter in the TC1 and TC2 settings. This parameter is indeed representative of the instrument including its response to stray light.

[43] *Aliwell et al.* [2002] have already pointed out the importance of using I_0-corrected cross sections. This correction takes into account the fact that the instrument has a finite resolution, whereas the observed structures, both solar and atmospheric, are highly structured. The finite resolution acts as a smoothing of the high-resolution structures, as they are convolved by the instrumental function. The problem arises when in equation (1) one uses absorption cross sections directly convolved by the instrumental function [*Hermans et al.*, 1999]. What should be done instead, in order to avoid the introduction of non-linear effects, is to use a corrected cross section defined by the following expression:

$$\sigma_{corrected}(\lambda) = \frac{1}{factor} \times \ln\left[\frac{synthetic(\lambda)}{solar(\lambda)}\right] \quad (2)$$

where *synthetic*(λ) is a synthetic spectrum calculated using high-resolution absorption cross sections and *factor* is the column amount of the target molecule, and then convolved with the low-resolution instrumental function; *solar*(λ) is the convolved solar Fraunhofer spectrum. I_0-correction factors were fixed to 2.5×10^{16} and 1.0×10^{20} for NO_2 and O_3, respectively.

[44] With each TC, two series of results were obtained corresponding to the use of either a daily reference spectrum or a single reference spectrum. When using a daily reference spectrum, small changes in the wavelength scale are more easily accounted for and corrected in the analysis procedure. However, the use of a single reference spectrum is often preferred for long-term analysis. The denominations TR0, TR1, and TR2 refer to their TC equivalents.

5. Comparison of Slant Columns

[45] One difficulty of the comparison resides in the relatively small observed NO_2 slant columns, smaller than 5.0×10^{16} molec/cm^2 at 95° sza during most of the days. However the main difficulty is the absence of independent NO_2 measurement by another technique to which those of the UV-visible spectrometers could be compared. The choice was to use a method suggested by *Roscoe et al.* [1999] for defining a reference based on objective criteria. The method is based on the analysis of the linear regression between different data sets of different groups. It allows a characterization of how well the two instruments' measurements agree together.

[46] First of all, the measurements are projected on a common solar zenith angle (sza) scale, varying from 75° to 95° with a 0.2° step. This was done by binning individual values taking into account their individual uncertainties. If $X = \{X_i\}$ and $Y = \{Y_i\}$ represent the measured slant columns of the two instruments interpolated on the common sza scale, the regression method best fits the slope (S) and intercept (I) parameters of the following equation:

$$Y = I + S \times X \quad (3)$$

[47] The linear regression yields a slope and an intercept for each pair of instruments. Ideally, those parameters should be 1.0 and 0.0. However, non-unity slope and non-zero intercept are expected as a consequence of the presence of systematic errors or differences between instruments. Using the slope and intercept, the offset and linear difference may be removed between the two selected data sets, defining residual values as

$$R_i = (I + S \times X_i) - Y_i \quad (4)$$

The evolution of these residuals vs sza gives moreover some insight into the dependence of the systematic difference on the sza. From the slope and intercept and from the evolution of the residuals with sza, a subgroup of instruments can be identified. These instruments may be considered as producing similar results and as such are being defined as the reference. This quantity is then obtained by averaging the subgroup data. An example of the procedure is presented in Figure 5. Figure 5a shows the regression analysis between each participating group and the NIWA_2 data for the 1st of March (TC0), and Figure 5b shows the residuals plotted against sza. From these graphs, the subgroup {IASB_1, INTA, IUPB_2, IUPH, NILU_2, NIWA_2} may be defined as the reference for this day as they best agree. Table 4 indicates which groups were considered as references for each TC. Unexpectedly, the groups were not the same for all TCs. It was however deemed necessary to consider the same groups as references for all TCs in order to avoid introducing biases in the interpretation of the regression and comparison results. Only those groups who had measurements for the three TCs, and were always in the chosen reference groups, were considered. This led to the final choice of the NO_2 reference:

$$ref_{NO_2} = Average\ of\ (IASB1\_1 + INTA + NIWA\_2)data \quad (5)$$

However, in the following, it must be kept in mind that this choice of reference does not mean that these measurements are the best. It just says that they best agree between themselves. Once the reference was defined, different types of comparisons were investigated:

[48] 1. Regression analysis against the defined reference provides a means for analyzing the nature of the disagreement existing between the various groups and the reference. The regression had to be applied to the largest sza interval possible in order to yield accurate intercept and slope. Data on the 75–95° sza interval were therefore considered. Regression parameters were determined by linear least square fitting, taking into account the uncertainties on the measured differential slant column densities. If $Y = \{Y_i\}$ and Ref = $\{\mathrm{Ref}_i\}$ represent, respectively, the measured slant columns of one instrument and the reference values interpolated on the common sza scale, and σ_i are the uncertainties associated with the Y_i measurements, the regression

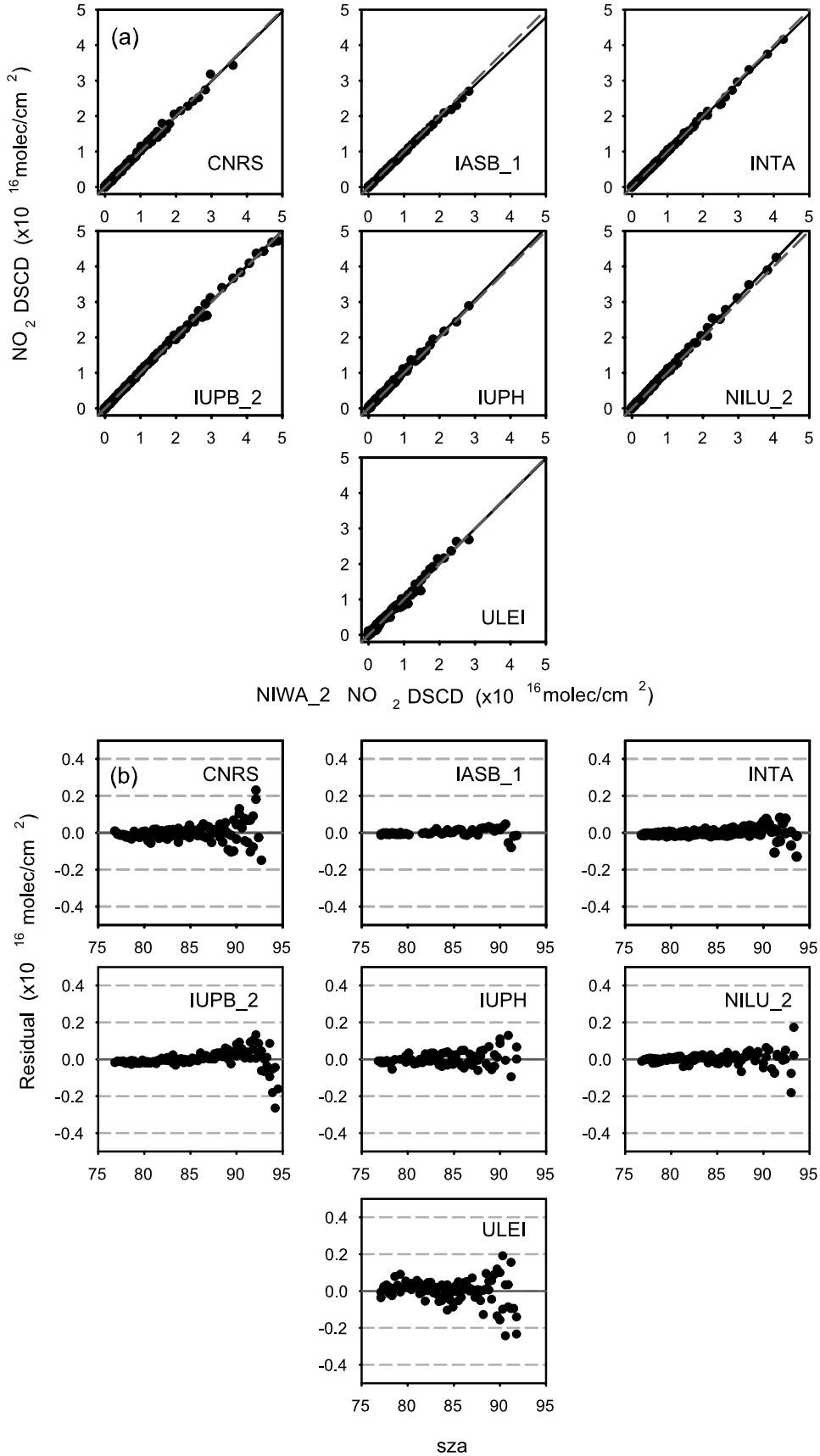

Figure 5. Illustration of the procedure used for selecting the NO_2 reference groups (TC0, day = March 1). (a) Regressions between measurements of each instrument and those of NIWA_2. The dashed line shows slope 1 and zero intercept. (b) Sza variations of residuals.

Table 4. Reference Groups for Each TC

TC	Reference Groups
TC0	IASB_1, INTA, IUPB_2, IUPH, NILU_2, NIWA_2
TC1	IASB_1, INTA, IUPB_2, NILU_2, NIWA_2
TC2	IASB_1, INTA, IUPH, NIWA_2

method best fits the slope (S) and intercept (I) parameters of the $Y_\sigma = I + S \times$ Ref equation.

[49] 2. Fractional differences $DSCDfd_i$ were also defined using the following relationship:

$$DSCDfd_i = \frac{DSCD_i - DSCD_{ref}}{DSCD_{ref}}(\%) \quad (6)$$

where $DSCD_i$ are the DSCD of group i and $DSCD_{ref}$ those of the reference. Uncertainties on the measured DSCDs were not taken into account. Average and standard deviation values were computed on restricted sza intervals. For sza below 80°, DSCD values are very small and relative differences become very large, even for small absolute differences.

[50] 3. Histograms of the DSCD differences were also plotted. They correspond to the distribution of values of the absolute differences between the DSCDs of one group and those of the reference. They illustrate some source of disagreement. The position of the distribution maximum provides an idea of the offset existing between one group and the reference, and its width illustrates the spread of data around the reference. Ideally, the maximum position should be as close as possible to zero and the distribution width should be as small as possible. A factor between two data sets will result in the distortion of the Gaussian type distribution. In order to visualize more clearly the origins of the discrepancies, two series of histograms were considered. In the first case, no corrections were applied to the instrument's data to be compared to the reference data. In the second case, the instrument's data were first corrected for the factor existing between both data sets, using the slope parameter derived from the regression analysis described earlier. Slope values for each half day were considered. In the following, these histograms will be referred to as the 'scaled histograms'. By combining both series of histograms, conclusions on the different effects, such as factor, offset and scatter of values, can be derived. Finally, histograms of the DSCD fractional differences were also investigated.

6. NO_2 Slant Columns

[51] Measurements of NO_2 DSCDs were performed by all groups. However, due to instrument limitations (mainly, the wavelength interval recorded), some instruments did not provide results for all TCs and TRs. Table 5 summarizes the available NO_2 data for each group and TC/TR. TC0 provided by some groups corresponded to either TC1 or TC2 (or TR), as indicated in the table.

[52] Figure 6 shows NO_2 DSCDs provided by all groups for three days: February 25 (high stratospheric NO_2 outside the vortex and polluted in the lower layers), February 26 (low NO_2 in the vortex in the evening and not polluted), and February 27 (in vortex but again polluted), and for the three TCs. Fractional differences for the same days are plotted in Figure 7. Some systematic differences between instruments and TCs can be observed. Fractional DSCD show them more clearly than the absolute DSCD, even if values at low sza are large as they correspond to the ratio of two small quantities. In general the spread of data is lower when using the TC1 settings and higher with the TC2 settings. Data of CNRS and ULEI show more short time variations. Moreover, the differences relative to the reference show no clear and systematic behaviors. For example, CNRS data in TC1 settings are about 25% lower than the reference on 25/02, and are evenly spread around it on 27/02. NILU data in TC0 mode seem to be about 10% higher than the reference, and those of IUPB in TC2 14% higher. All these rather crude observations will be analyzed in detail in the following sections.

6.1. Regression Analysis

[53] As said earlier, a regression analysis was performed: (1) daily for sunrise and sunset separately, (2) average for sunrise and sunset, and (3) overall average. This led to different sets of parameters for each group, consisting of the intercept and slope, with their uncertainties, and a rms residual. From the analysis of the daily values, which give information on the day to day variability of the NO_2 retrieval for each instrument, no systematic variation in time could be observed, such as for example a continuous drift of the offset or of the slope, which could be due to instrument instability. Regression performed on all days, distinguishing or not between am and pm values, led always to over-optimistic values of the parameters. This is probably due to the averaging of differences, which as already said, were not systematic. In other words, data from a day where DSCDs were over-estimated cancelled out data from days where DSCDs were under-estimated. It was then chosen preferable to base the comparison on daily regression parameters. Average values and standard deviations of the daily regression parameters were therefore calculated for each instrument. They are given in Table 6 in the case of the TC0 settings. On average over all the campaign, all instruments with their respective specific arrangements (TC0), meet with the NDSC Type I criteria (Slope = 1 ± 0.05, Intercept = $\pm 0.15 \times 10^{16}$ molec/cm^2 and Residual $< 0.10 \times 10^{16}$ molec/cm^2).

[54] Values of the intercept and rms residuals are lower than those obtained during the last intercomparison campaign held at the Observatoire de Haute Provence [*Roscoe et al.*, 1999]. A closer look at the regression parameters obtained by *Roscoe et al.* [1999] shows that the present intercept values are about a factor of 4 lower than those at OHP (Observatoire de Haute Provence). However, the OHP

Table 5. List of TC Data Provided by Each Group

Group	TC0	TC1	TC2	TR0	TR1	TR2
CNRS	X	X	-	X	-	-
IASB	TC1	X	X	TR1	X	X
INTA	TC1	X	X	TR1	X	X
IUPB	X	X	X	X	X	X
IUPH	TC2	-	X	TR2	-	X
NILU	X	X	-	X	X	-
NIWA	X	X	X	X	X	X
ULEI	X	X	X	-	-	-

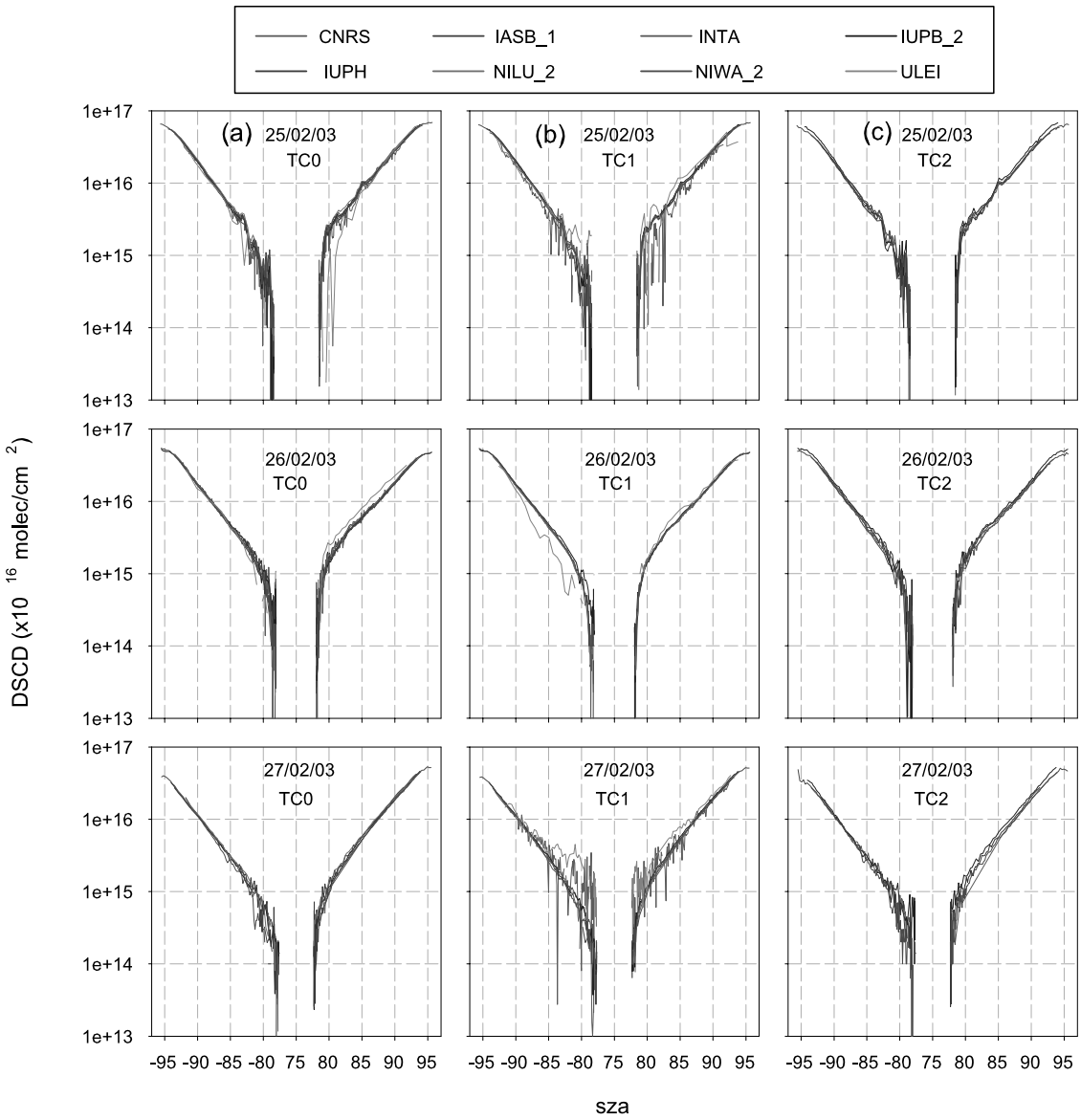

Figure 6. NO_2 DSCDs measured by all groups on February 26, 27, and 28 for (a) TC0, (b) TC1, and (c) TC2 settings. The color code is also given on the figure. See color version of this figure at back of this issue.

reference spectrum corresponded typically to a sza lower than 30°, while the Andøya reference spectra were obtained near 75°. With the twilight interval starting at 70 or 75 degrees, there is a larger uncertainty on the determination of the intercept during the OHP campaign. The better intercepts can then be understood as resulting from the smaller sza range observed in this study. Comparison of the slope values shows an improvement of a factor of 2 when considering only the groups which best agreed. The largest improvement is observed for the residuals, with a factor almost equal to 10, again when considering only the groups included into the respective references. This is to be related to a series of different factors, such as (1) improvements realized both in the instrumentation and the retrieval algorithms, (2) the limited sza range and the short duration of polar days, (3) low tropospheric NO_2 signals, and (4) the small contribution of the Ring effect in the recorded spectra, due to the small sza amplitude and to the presence of a dense and generally stable cloud layer. All above effects have a positive influence on the measurements quality, as they minimize the sources of systematic errors. However, it should be noted that the presence of the dense cloud layer also causes a diminution of the light level and that the NO_2 columns measured during the Andøya campaign were rather small (typically lower than 4×10^{16} molec/cm^2, compared to values of up to 12×10^{16} molec/cm^2, at large sza for mid-latitude summer conditions as encountered during the NDSC campaign of the Observatoire de Haute Provence). These effects all result in a reduction of the signal-to-noise ratio of the observations. Favorable factors seem however to have been more important, leading to lower residuals on the retrieved NO_2 amounts.

[55] Slope deviations from unity are smaller than 5% for all groups, when considering values obtained by averaging

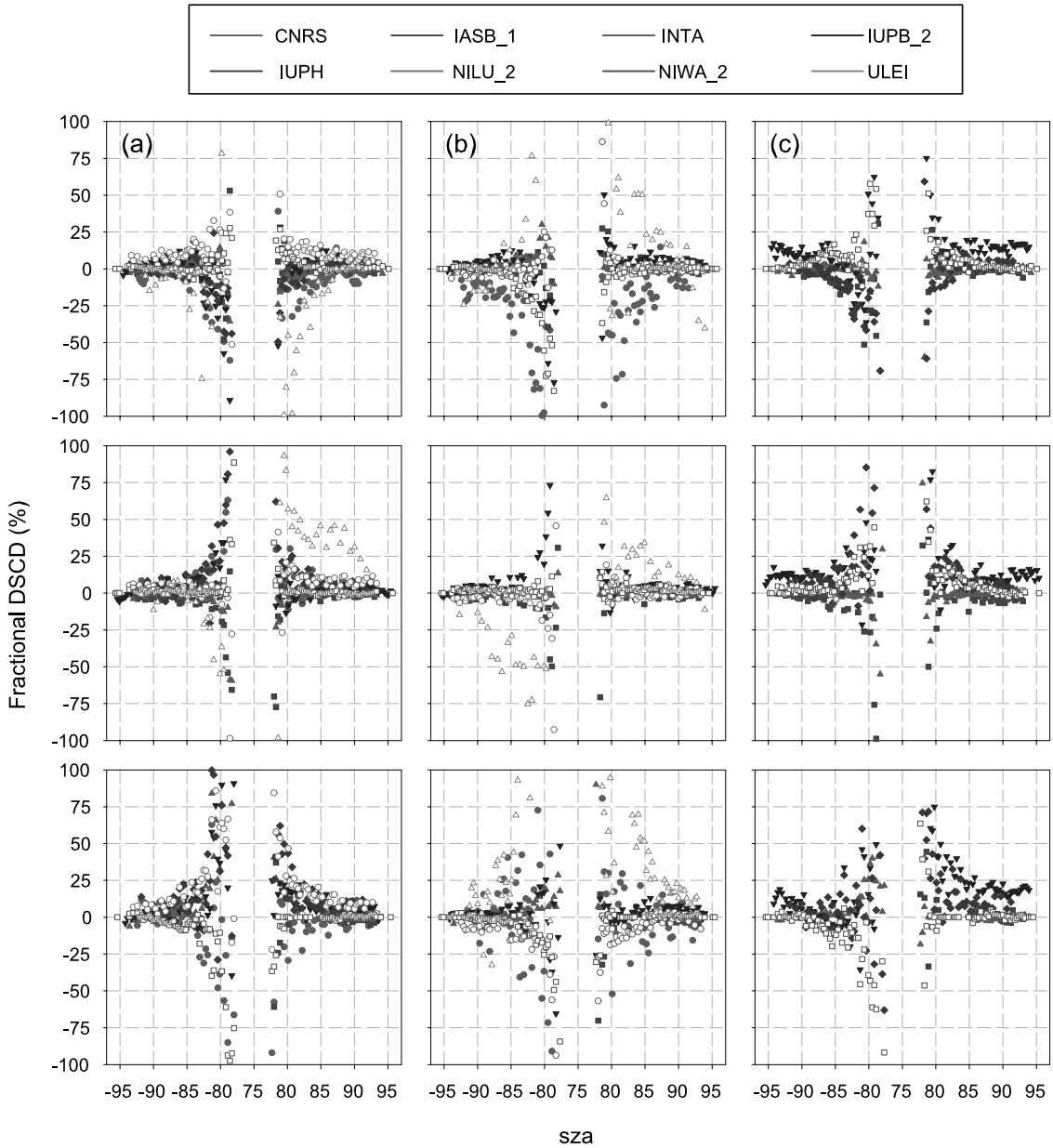

Figure 7. NO_2 fractional differences for all groups on February 26, 27, and 28 for (a) TC0, (b) TC1, and (c) TC2 settings (solid circles, CNRS; solid squares, IASB_1; solid triangles, INTA; solid inverted triangles, IUPB_2; solid diamonds, IUPH; open circles, NILU_2; open squares, NIWA_2; open triangles, ULEI). See color version of this figure at back of this issue.

all daily (am and pm) slopes. However a closer look at the results shows that the behavior of the slope differs quite largely in the am and pm data. In general, average daily am slopes are closer to unity, but with higher standard deviations, and the reverse (larger deviation from unity, smaller standard deviation) is observed for the average pm slopes. This can be understood by going back to the daily regression parameters. For am, the daily slopes are much more varying but are evenly spread around 1.0. In contrast, the pm daily slopes are far less varying but generally differ more from unity. Those results can be related to the fact that generally am DSCDs are smaller at large sza, narrowing the interval on which the regression is applied, thus leading to much less defined slopes. The slope uncertainty, coming out of the regression analysis, is thus larger in the am than at pm.

[56] Table 7 shows the slopes of the regression for TC0, TC1, and TC2. The results are similar but on a few points.

[57] 1. If TC1 is considered, almost all instruments comply with the NDSC criterion (slope 1.00 ± 0.05), only ULEI showing a larger standard deviation. However, the use of only these numbers as criterion might in certain cases be misleading, as illustrated by the results from the ULEI instrument. A closer look at the average slopes for am and pm periods separately (see Table 6, for example), shows that the discrepancies are quite different for the two periods.

Table 6. Results of the Regression Analysis for TC0: Average Daily Intercept (I), Slope (S), and rms Residual (R) With Their Standard Deviations for Each Instrument for Sunrise (SR), Sunset (SS), and (SR+SS)

		TC0					
		I, $\times 10^{13}$ molec/cm^2		S		R, $\times 10^{13}$ molec/cm^2	
		Mean	Std. Dev	Mean	Std. Dev	Mean	Std. Dev
CNRS	SR	0.1	28.3	1.013	0.043	6.6	1.8
	SS	2.3	18.1	1.008	0.031	8.9	3.6
	SR+SS	1.1	23.3	1.010	0.038	7.7	3.0
IASB	SR	−0.1	8.7	0.992	0.024	3.1	1.4
	SS	−4.2	8.7	0.989	0.007	4.4	2.8
	SR+SS	−1.8	8.7	0.990	0.017	3.8	2.3
INTA	SR	1.8	6.4	0.997	0.026	3.4	1.5
	SS	0.1	11.5	0.993	0.006	3.2	1.1
	SR+SS	1.1	9.0	0.994	0.020	3.3	1.3
IUPB	SR	3.1	11.6	1.022	0.032	8.7	4.1
	SS	1.2	8.4	1.045	0.009	10.7	3.4
	SR+SS	2.4	10.0	1.036	0.024	9.7	3.8
IUPH	SR	−1.0	13.5	1.032	0.035	4.5	1.1
	SS	−6.4	18.5	1.014	0.025	4.8	1.2
	SR+SS	−3.7	15.8	1.019	0.034	4.6	1.1
NILU	SR	3.1	18.9	1.039	0.041	7.9	4.3
	SS	1.8	14.5	1.062	0.028	9.6	4.6
	SR+SS	2.5	16.5	1.053	0.035	8.8	4.4
NIWA	SR	−2.1	5.5	1.003	0.013	3.2	1.3
	SS	0.1	6.9	1.008	0.007	3.5	1.5
	SR+SS	−1.1	6.3	1.006	0.012	3.4	1.4
ULEI	SR	−3.6	16.2	0.903	0.055	10.6	4.9
	SS	14.6	55.0	1.056	0.083	13.4	5.6
	SR+SS	5.6	39.0	1.027	0.118	12.0	5.3

The average slopes of ULEI instrument are 10% smaller in the am, but 6% higher at pm. However, by averaging am and pm, these effects cancelled out, resulting in a better average slope, but with admittedly a high standard deviation value.

[58] 2. The performance of all instruments degrades using TC2. This is particularly true for IUPB_2 NO_2 for which the DSCDs are about 14% larger than the reference when using the TC2 settings. This systematic behavior is observed every day and more pronounced for pm periods. No clear reason could be found to explain such high differences.

[59] 3. A significant drop of 6.7% and 6.0 % respectively could be observed between TC0 and TC1 for the two instruments, CNRS and NILU, showing also the largest TC0 slopes in Table 6 and performing at longer wavelengths than others. The main reason for that is the larger Air Mass Factor (AMF) at large sza at longer wavelengths resulting in a faster growth of the NO_2 slant column (though of smaller amplitude in the polar vortex). This results in a steeper slope of regression compared to the reference and thus in a positive deviation in the fractional difference at high sun in the absence of pollution as shown in Figure 7 on February 26, and in the opposite in case of pollution at warm temperature as on February 25 and 27 on the same figure.

[60] 4. The CNRS TC1 is aliased with respect to TC0 because of the lower sampling ratio and larger spectral range of the instrument, resulting in a reduced signal to noise when using a restricted spectral range.

[61] The same analysis was performed on the data retrieved using one single reference spectrum for all days. This single reference was chosen to correspond to the spectrum with the lowest sza recorded on the March 5. The ULEI instrument could not provide such data as it appeared not to be stable enough throughout the campaign. The instrument was still in test mode and its configuration, e.g., the grating position, and in turn the spectral interval recorded, was varied for optimizing the settings. The use of a single reference spectrum had no influence on the average of SR and SS slopes and residuals, and on their standard

Table 7. Average (SR+SS) Slopes and Standard Deviations for the Three TCs

	TC0		TC1		TC2	
	S	Std. Dev.	S	Std. Dev.	S	Std. Dev.
CNRS	1.010	0.038	0.946	0.050	-	-
IASB	0.990	0.017	0.990	0.011	0.990	0.022
INTA	0.994	0.020	0.995	0.010	1.001	0.018
IUPB	1.036	0.024	1.035	0.019	1.140	0.049
IUPH	1.019	0.034	-	-	1.033	0.020
NILU	1.053	0.035	0.993	0.020	-	-
NIWA	1.006	0.012	1.010	0.007	1.003	0.012
ULEI	1.027	0.118	0.981	0.107	1.065	0.100

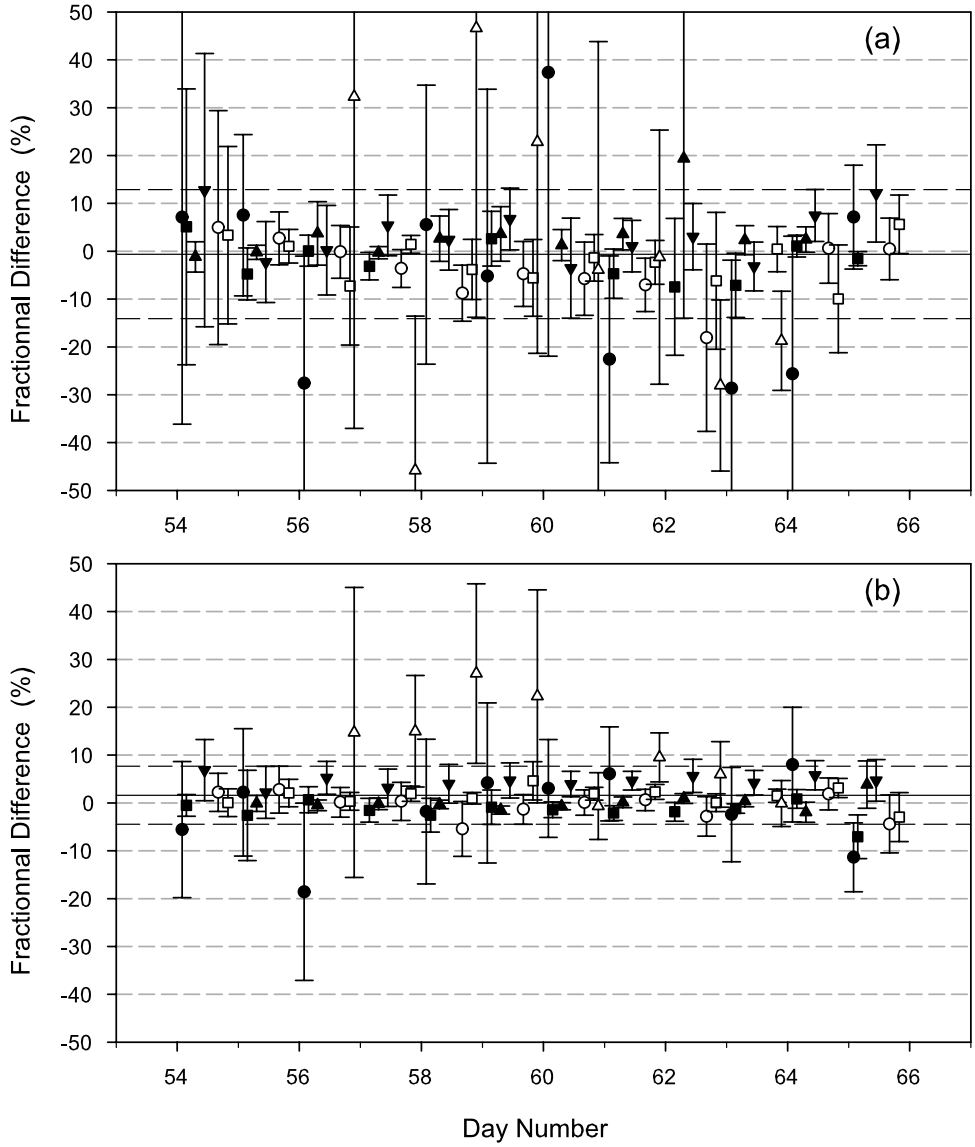

Figure 8. Daily (a) am and (b) pm averages of the fractional differences for all groups and TC1 settings. The error bars represent the standard deviation (solid circles, CNRS; solid squares, IASB_1; solid triangles, INTA; solid inverted triangles, IUPB_2; solid diamonds, IUPH; open circles, NILU_2; open squares, NIWA_2; open triangles, ULEI).

deviations. The intercept values, however, were always higher, at least for the instruments not included in the reference. The average of am and pm values was a factor 10 larger, while the standard deviations were 2 times higher than those obtained with daily reference spectra. However, they were still always much smaller than 5.5×10^{14} molec/cm^2 and 8.0×10^{14} molec/cm^2 in the am and pm, respectively.

6.2. Fractional Differences

[62] Figure 7 suggests that it could be more appropriate to consider only the fractional differences for sza larger than 80° since below this limit, little information could be gained on the relative performance of the instruments. Figure 8 shows the daily fractional differences and their standard deviations for all instruments during the full campaign using the TC1 spectral range compared to the campaign average including all instruments represented by horizontal lines (top: am; bottom: pm). A difference between SR and SS clearly appears: pm values being far less variable for all instruments. The global mean and standard deviation are also indicated on each graph, obtained by taking into account all values for all instruments and all days. The global mean is always around zero, but the standard deviation greatly differs: from 13.5% in am data to 6% in pm measurements. As already shown above, two instruments, CNRS and ULEI, are displaying larger deviations.

[63] In Figure 8, all instruments were considered when determining the global standard deviation. It is however interesting to investigate what happens to this quantity when some instruments are removed from the calculation. Figure 9 represents the global standard deviation, or spread of data, for different groups of instruments for all three TCs. The

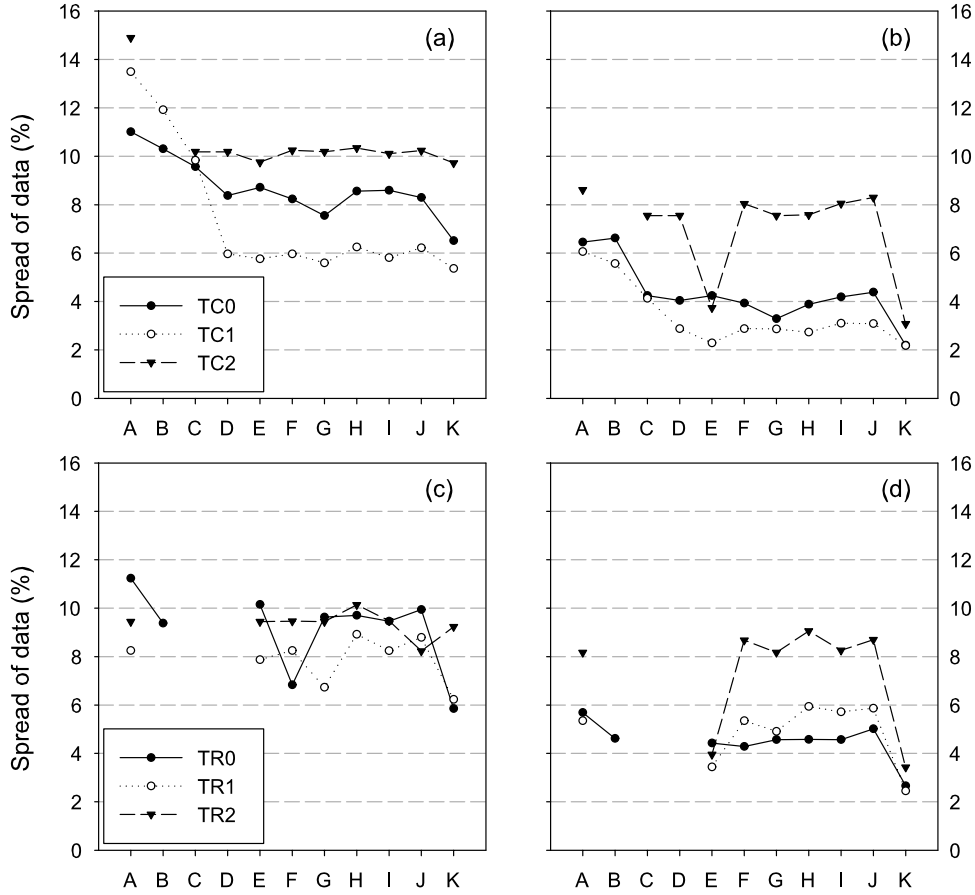

Figure 9. Evolution of the standard deviation for the three settings: (a) am and (b) pm with a daily reference spectrum, and (c) am and (d) pm using a single reference spectrum during the whole campaign. A, all instruments; B, all instruments – CNRS; C, all instruments – ULEI; D, all instruments – CNRS – ULEI; E, D – IUPB_2; F, D – IUPH; G, D – NILU_2; H, D – IASB_1; I, D – INTA; J, D – NIWA_2; K, the reference groups (IASB_1, INTA, and NIWA_2).

different cases correspond to A: All instruments; B: All instruments – CNRS; C: All instruments – ULEI; D: All instruments – CNRS – ULEI; E: D – IUPB_2; F: D – IUPH; G: D – NILU_2; H: D – IASB_1; I: D – INTA; J: D – NIWA_2; and K: the reference groups (IASB_1, INTA, and NIWA_2). Am and pm values are plotted separately in Figures 9a and 9b respectively for the analysis with daily reference spectra, and in Figures 9c and 9d when a single reference spectrum is used instead throughout the campaign. The behavior is similar for all TCs; however, the levels of spread of data are quite different. In general, a plateau is attained after the removal of CNRS and ULEI data. Then removing one instrument (cases E → J) or more (case K) does not change the global standard deviation. The lower spread of data, which also corresponds to the best agreement between the instruments, is obtained when using the TC1 imposed parameters. In this case, an agreement of 6% for am and 3% for pm values is obtained leading to an overall 5% agreement when considering all am and pm data. The decrease after removing the CNRS and ULEI results is less pronounced for the TC0 settings. In this case, a general agreement of 7% is attainable. However a value of 5% is reached when considering only the reference groups. For TC2, the evolution of the global standard deviation is different at am and pm, reinforcing the fact that IUPB_2 TC2 values show a more pronounced systematic divergence during the pm periods. If the IUPB_2 results were to be removed as well from the calculation, the overall pm agreement between the remaining instruments would be of the same order of the one obtained with the TC0 settings. Figures 9c and 9d show that the three TRs (same as TCs but using a single reference spectrum) perform quite similarly. They all give rise to an agreement lying between 7 and 10% for am, and, if IUPB_2 data are removed, around 5% for pm.

[64] As expected, the differences between the instruments vary greatly with the sza interval investigated. For example if we consider the global standard deviation obtained for the pm values of all instruments except CNRS and ULEI, the variation is the following: 22% on the 75–80°, 5% on 80–85°, 2.7% on the 85–90°, and 2.1% on the 90–95° sza interval. This variation is mainly due to the fact that the DSCDs are larger at high sza while the divergence between instruments remains of the same order.

6.3. Histograms

[65] Histograms of DSCD differences are another means to illustrate the differences existing between instruments. As already discussed, two types of histograms of DSCD differences were considered in this work, using scaled

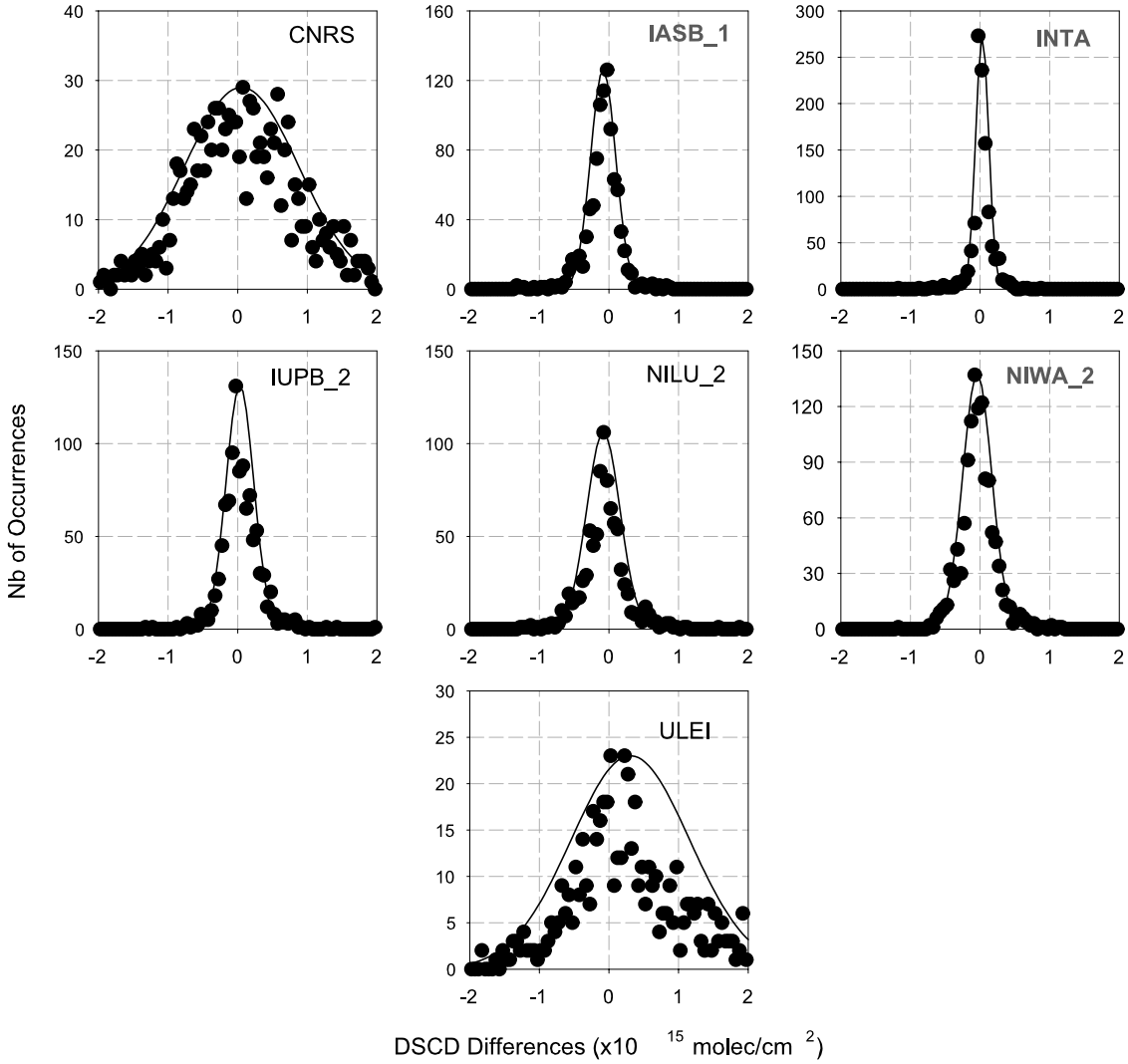

Figure 10. Histograms of DSCD differences for each instrument compared to the reference for TC1. The abscissa are the absolute differences observed between one instrument and the references, and the y-axis represent the number of occurrences of one specific difference value. The solid line shows the normal function of the same mean and standard deviation as the data.

and non-scaled DSCD values. In both cases, DSCDs corresponding to sza comprised between 75 and 92° and acquired from February 23 up to March 6 were included in the calculations. Figure 10 presents the scaled histograms for each instrument for the TC1 settings. The number in ordinate is the number of occurrences of a given difference between the DSCDs of one instrument and those of the reference. If these differences are totally random and the instrument or the retrieval are not biased, the distribution should be Gaussian. The distributions associated to the reference groups are of course narrower and with a maximum position closer to zero. As expected, CNRS and ULEI distributions are broader, corroborating the greater variability of those measurements. The IASB_1, INTA and NIWA_2 instruments produce narrower DSCDs distributions, which is expected as they define the reference. Comparison between scaled and non-scaled histograms give some information on the response of some instruments. For example, the non-scaled histogram of the IUPB_2 results shows a positive bias, almost defining a second maximum, which completely disappear when considering the scaled values. This clearly indicates that the observed bias is due to a factor and not an offset. These data however correspond to TC1 and not TC2 settings. From the histograms, it seems that the bias observed in TC2 might already be present in the other TCs.

[66] To better characterize these distributions, a detailed analysis of their properties has been performed, by computing their mean, standard deviation, median, skewness, and kurtosis. The skewness is a measure of the asymmetry of the distribution, while the kurtosis represents the degree to which the distribution is flattened with respect to a normal curve. These two quantities are related to the 3rd and 4th moment of the distribution respectively. A positive value of the skewness signifies a distribution with an asymmetric tail extending out towards more positive values of the independent variable, while a negative value corresponds to a distribution having a tail extending out towards

Table 8. Statistics of the Histograms of DSCD Differences for the Three Test Cases: Total Number of Occurrences (N), Mean, Standard Deviation, Median, Skewness, and Kurtosis[a]

Group	N	Mean, $\times 10^{13}$ molec/cm^2	Std Dev, $\times 10^{14}$ molec/cm^2	Median, $\times 10^{13}$ molec/cm^2	Skewness	Kurtosis
TC0						
CNRS	1124	3.15	3.96	0.00	0.09	4.12
IASB_1	902	−7.63	1.73	−10.00	−0.81	5.40
INTA	1010	5.34	1.54	0.00	0.29	4.41
IUPB_2	1004	6.41	2.20	0.00	−1.72	22.43
IUPH	779	−2.69	2.97	−5.00	0.92	4.45
NILU_2	864	1.86	2.76	0.00	−0.92	11.77
NIWA_2	1139	−6.36	1.49	−10.00	0.56	3.47
ULEI	464	−6.30	6.41	−5.00	−1.08	2.38
TC1						
CNRS	951	5.69	8.24	0.00	−0.05	1.71
IASB_1	907	−8.35	1.81	−10.00	−0.68	4.27
INTA	991	3.21	0.93	0.00	−0.95	9.05
IUPB_2	980	3.28	1.99	0.00	0.38	13.00
NILU_2	854	−8.02	2.41	−10.00	0.49	12.06
NIWA_2	1157	−3.93	2.09	−5.00	0.60	2.23
ULEI	538	30.87	8.51	20.00	0.27	1.98
TC2						
IASB_1	897	−16.75	2.64	−15.00	0.07	2.37
INTA	990	−0.38	1.18	−5.00	1.07	6.86
IUPB_2	1012	−8.29	3.45	−10.00	0.70	3.84
IUPH	774	−7.22	3.36	−5.00	−0.07	1.43
NIWA_2	1170	−1.68	2.95	−5.00	−0.25	0.88
ULEI	314	51.32	10.00	10.00	0.83	0.12

[a]See text for the definition of these parameters.

the more negative values of the independent variable. Kurtosis measures the flatness of the curve. If its value is negative, the distribution is flatter in the vicinity of the maximum than the normal curve. A positive value implies a distribution that is more sharply peaked. Table 8 summarizes these parameters for the distributions of the DSCD differences for the three test cases. Looking at both this table (TC1 results) and Figure 10, it can be concluded that, except in the case of ULEI, the distributions are quasi-symmetrical (skewness near zero).

[67] Histograms of the DSCD fractional differences have also been investigated, by plotting the distributions for each participating instrument and by computing the different parameters describing mathematically those distributions. Figure 11 illustrates the distributions obtained in the case of the TC1 test case, while Table 9 summarizes the statistical parameters for the three test cases. The mean value and the standard deviation give information on the offset between one instrument and the reference and the spread of points around these values, which have already been discussed earlier. From Table 9 and Figure 11, it can be seen that the CNRS instrument is quasi-symmetrical, that the INTA and ULEI instruments both show an extending tail towards the positive DSCD differences, while all the remaining instruments show the opposite behavior. Considering the kurtosis parameter, INTA has the more peaky distribution, while the CNRS and ULEI the more flattened.

6.4. Impact of Choice of the NO_2 Absorption Cross Sections

[68] High-resolution absorption cross sections of NO_2 are available in the literature at different temperatures [*Harder et al.*, 1997; *Vandaele et al.*, 1998]. Both sets were obtained with Fourier transform spectrometers leading to a very accurate wavelength calibration. Using the cross section of *Harder et al.* [1997] at 227 K and 294 K, instead of those of *Vandaele et al.* [1998] at 220 K and 294 K, leads to a systematic difference of 7 % in the retrieved NO_2 column [*Carleer et al.*, 2001]. Some of this difference is caused by use of different low temperature cross sections in the analysis and does not seems to be related to the quality of either of the cross sections or the analysis algorithms. The impact of the different temperatures at which those cross sections are reported has been further analyzed by the NIWA group. NIWA spectra for March 5 covering the SZA range 95.76° AM to 95.92° PM, were processed using the *Harder et al.* 227 K NO_2 cross sections for TC1 conditions (425–450 nm). The results were compared by linearly regressing column NO_2 results obtained using the *Vandaele et al.* cross sections on those obtained using the *Harder* cross sections to attain, slope = 0.9538 ± 0.0002 and intercept = $-9.6 \times 10^{12} \pm 3.1 \times 10^{12}$ molec/cm^2, a fractional difference of about 4.6%. To correct for the cross section temperature difference, the *Vandaele* 294 K differential cross section was regressed on *Vandaele* 220 K cross section to obtain, slope = 0.779 and intercept = 1.3×10^{-21} molec/cm^2. These two cross sections were converted to differential cross sections by subtracting the best fit second-order polynomial, before doing this regression, to better model typical analysis algorithms. Assuming the temperature dependence to be linear, the fractional change between 220 K and 227 K is therefore = 0.0209, or about 2.1%. This results in a temperature corrected column NO_2 results comparison coefficient = 0.9747, equivalent to a difference of about 2.5% with the use of the *Harder* cross sections producing the larger values. This is within the stated cross section accuracies of 3% for the *Vandaele* cross sections and 4% for the *Harder* cross sections. The spectral residuals using either *Vandaele* or *Harder* cross sections on

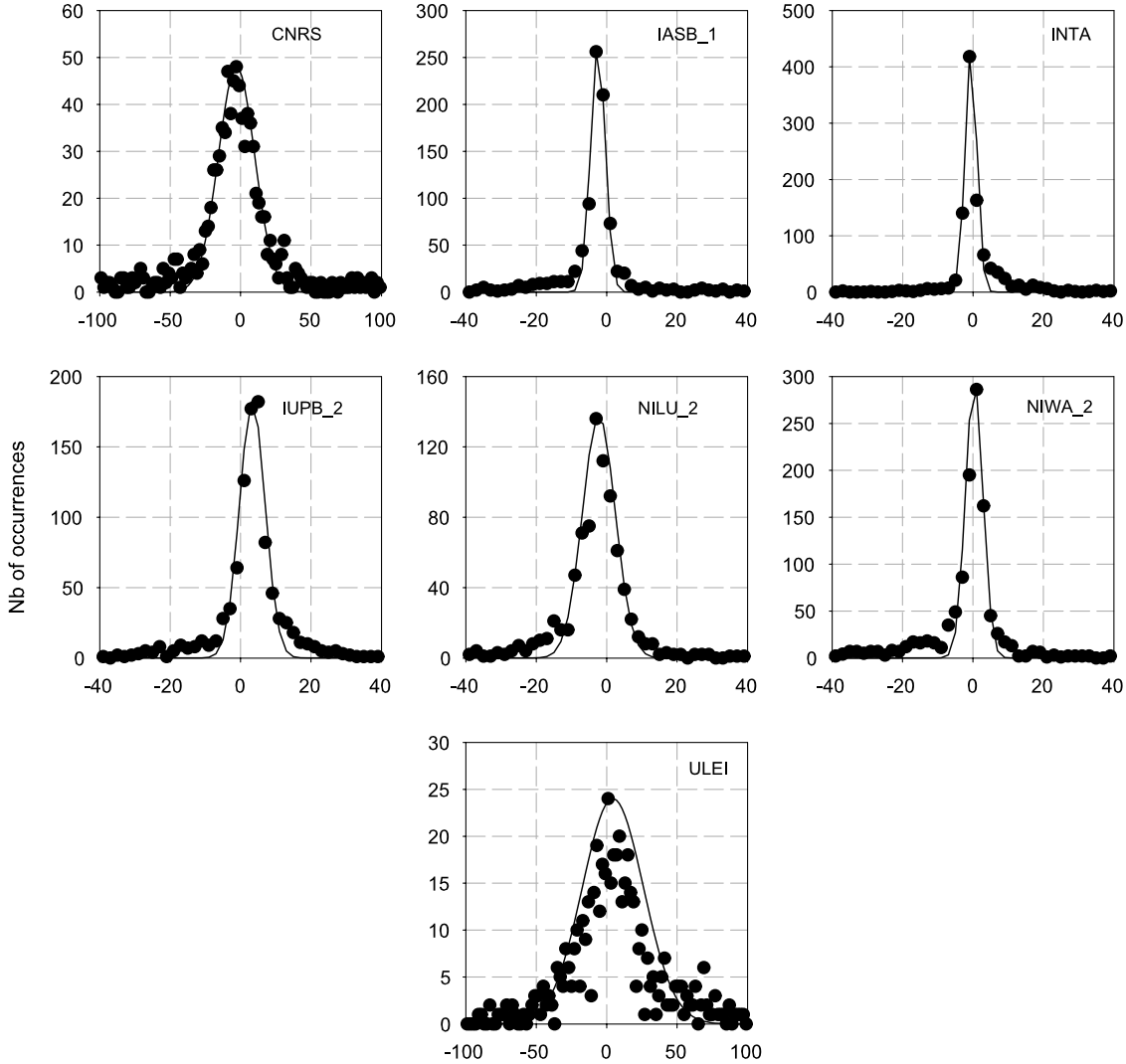

Figure 11. Same as Figure 10, but in relative differences. Note the different x scale for CNRS and ULEI.

this data set were essentially the same. In his review of the existing NO_2 absorption cross sections [*Orphal*, 2002], *Orphal* concludes with some recommendation for the choice of the NO_2 cross sections to use in atmospheric remote-sensing studies. Cross section of *Vandaele et al.* [1998] at 220 and 294 K were recommended as a standard for the 240–790 nm region, along with a linear model to interpolate for intermediate temperatures.

[69] Since most of instruments have adopted the *Vandaele et al.* cross-sections at 220 K, the derived NO_2 slant columns should agree within the experimental errors on the cross sections. In the case of NILU TC0 using the *Harder et al.* data at 227 K, derived NO_2 slant columns are expected to be 4.6% higher relative to the other analyses, because of the use of different cross sections.

6.5. Impact of Interfering Species

[70] The O_3 temperature-dependent cross sections of *Bogumil et al.* [2000] had been considered by all groups. Since the temperature dependence of the ozone absorption in the visible Chappuis bands is smaller than 1%, it was not deemed necessary to take more than one temperature (223 K) into account.

[71] The O_4 absorption cross-sections of *Greenblatt et al.* [1990], after correction for shift and stretch, are used by most of the groups. The data of *Hermans et al.* [2002] are not recommended in this region, as they contain a small artifact, which is not found in the spectra of *Greenblatt et al.* [1990], nor in the atmosphere.

[72] The 441–449 nm region includes weak water vapor absorptions bands with a peak near 442.8 nm between two NO_2 bands, first identified by *Curcio et al.* [1955], and measured later by *Camy-Peyret et al.* [1985], which may have an impact on the NO_2 measurement. Most of the groups are using the water vapor line parameters listed in the HITRAN 2000 database [*Rothman et al.*, 2003] except NIWA who is using high resolution FTS measurements of actual atmospheric water vapor absorption measured at the National Solar Observatory, Kitt Peak, Arizona by *Harder and Brault* [1997]. Indeed those were found to significantly improve the accuracy of the fitting of water vapor absorption. This is consistent with recent measurements by *Coheur*

Table 9. Same as Table 8, but for Relative Fractional Differences

Group	N	Mean, %	Std Dev, %	Median, %	Skewness	Kurtosis
TC0						
CNRS	902	0.53	8.34	0.00	−1.09	4.79
IASB_1	692	−2.42	2.73	−4.00	−1.00	10.73
INTA	806	−0.35	2.81	−2.00	−0.45	10.96
IUPB_2	789	4.22	4.40	2.00	−0.71	9.24
IUPH	636	1.87	9.08	0.00	−0.45	5.06
NILU_2	682	6.22	5.88	4.00	0.08	5.55
NIWA_2	918	−1.03	3.08	−2.00	0.14	12.16
ULEI	381	−2.34	21.96	0.00	−0.01	1.79
TC1						
CNRS	770	−4.10	16.42	−4.00	0.01	2.30
IASB_1	677	−2.49	2.07	−4.00	−0.74	11.45
INTA	829	−0.32	2.02	−2.00	0.83	19.67
IUPB_2	793	3.63	3.93	2.00	−1.14	9.72
NILU_2	708	−2.67	4.97	−4.00	−0.98	10.82
NIWA_2	858	0.06	2.81	0.00	−0.94	8.72
ULEI	431	4.33	23.83	2.00	0.22	0.50
TC2						
IASB_1	721	−4.00	4.25	−4.00	−1.30	8.83
INTA	733	−0.72	1.62	−2.00	0.79	11.80
IUPB_2	801	10.93	10.95	10.00	−0.69	2.76
IUPH	593	2.26	7.58	2.00	−1.24	4.15
NIWA_2	846	−0.04	4.02	−2.00	−0.49	5.25
ULEI	267	10.24	23.76	6.00	0.26	1.84

et al. [2002] showing the presence of a number of additional small lines not yet included in the HITRAN database.

7. Conclusions

[73] A third intercomparison of UV-visible zenith-sky instruments has been conducted in the framework of the Network for the Detection of Stratospheric Changes (NDSC). For the first time it was held at high latitude in winter and therefore is representative of polar areas. The campaign took place at the Andøya Rocket Range at Andenes (Norway, 69°N, 16°E) from February 21 to March 6. Eight international groups with twelve instruments participated in the campaign. Eleven of the instruments are commonly used at NDSC stations and one, of the University of Leicester, is a new instrument still under development. Though the high latitude site permitted also the comparison of BrO and OClO, only the results obtained for NO_2 are presented here.

[74] The data submitted by each group, before seeing the results of the others, were analyzed by a regression technique, where the results of each group were compared to those of a reference following a method proposed by *Hofmann et al.* [1995], later improved by *Roscoe et al.* [1999] by the use of a common reference made of a combination of instruments performing comparably. Here, the reference was built from measurements of three instruments showing consistent agreement among each other. Besides the use of regression analysis, the differences in measurements were highlighted through the analysis of fractional differences relative to the reference, and histograms of the absolute and fractional differences in measurements. Different sets of analysis parameters (TC) were investigated, which allowed a better characterization of the differences between instruments.

[75] Almost all instruments agreed within 5% or better, when the analysis parameters are imposed, and using the 425–450 nm spectral interval (TC1). This agreement degrades to 9% when retrieving NO_2 in the 400–418 nm region and to 7% if each group uses its preferred choice of parameters. The analysis shows that most of the instruments comply with the NDSC selection criteria under polar conditions, the newly developed spectrometer of the University of Leicester sometimes showing larger deviations. Among the others, the CNRS spectrometer which uses a wider spectral range extending to longer wavelengths shows the largest differences with the reference.

[76] The results of the regression analysis discussed in this paper have been compared to those obtained during the previous NDSC campaign [*Roscoe et al.*, 1999]. It has been shown that when considering the groups with best agreement (1) no obvious improvement as regards the intercepts was gained; (2) an improvement of a factor 2 at best has been achieved as regards the slopes; and (3) significant improvement has been achieved as regards the residuals (a factor of almost 10), probably due to the more restrained DOAS analysis settings and the generally more stable measurement conditions at Andøya. Globally, much better general agreement between all groups was observed.

[77] On the basis of the results of the comparison, several recommendations can be made:

[78] 1. The same NO_2 absorption cross-section of, e.g., *Vandaele et al.* [1998] should be used for the analysis of all instruments. This cross section has already been adopted by most groups.

[79] 2. Correction for water vapor absorption should be improved as it can interfere significantly with the NO_2 retrieval. The HITRAN database does not currently provide accurate enough information, and also the atmospheric cross section of *Harder and Brault* [1997] do not fit perfectly for all measurement conditions.

[80] 3. Using the wavelength interval of 400–418 nm as suggested by *Preston et al.* [1997] leads to larger differences between results of different instruments and is therefore not recommended.

[81] Finally, it could be concluded that better consistency between NDSC stations could be achieved by using instruments of similar design, wavelength ranges and data analysis algorithms. However, this is not recommended, since it would not necessarily improve the accuracy of the measurements, and could result in the masking of several issues not yet totally solved.

[82] **Acknowledgments.** First of all, we would like to thank M. Gausa, K. Bekkelund, R. Lyngra, and the personnel of the Andøya Rocket Range Facility and the ALOMAR center for their help in organizing the campaign. The financial funding from ARI is also acknowledged. The NIWA authors would like to acknowledge the large technical contribution by Alan Thomas and John Robinson in building and calibrating the spectrometers, and the travel support provided by the EU.

References

Aliwell, S. R., et al. (2002), Analysis for BrO in zenith-sky spectra: An intercomparison exercise for analysis improvement, *J. Geophys. Res.*, *107*(D14), 4199, doi:10.1029/2001JD000329.

Bogumil, K., J. Orphal, and J. P. Burrows (2000), Temperature-dependent absorption cross-sections of O_3, NO_2, and other atmospheric trace gases measured with the SCIAMACHY spectrometer, paper presented at ERS-ENVISAT Symposium, Eur. Space Agency, Gothenburg, Sweden.

Burrows, J. P., A. Dehn, B. Deters, S. Himmelmann, A. Richter, S. Voigt, and J. Orphal (1998), Atmospheric remote-sensing reference data from GOME: part 1. Temperature-dependent absorption cross-sections of NO_2 in the 231–794 nm range, *J. Quant. Spectrosc. Radiat. Transfer*, *60*(6), 1025–1031.

Camy-Peyret, C., J.-M. Flaud, J.-Y. Mandin, J.-P. Chevillard, J. Brault, D. Ramsay, M. Vervloet, and J. Chauville (1985), The high-resolution spectrum of water vapor between 16,500 and 25250 cm^{-1}, *J. Mol. Spectrosc.*, *113*, 208–228.

Carleer, M., C. Fayt, A. C. Vandaele, and M. Van Roozendael (2001), Choosing an NO_2 cross-section for UV-Vis atmospheric measurements: Impact on NO_2, BrO, OClO, . . . concentration retrievals, paper presented at Workshop on Laboratory Needs for Atmospheric Sensing, San Diego, Calif., 22–26 Oct.

Coheur, P.-F., S. Fally, M. Carleer, C. Clerbaux, R. Colin, A. Jenouvrier, M.-F. Mérienne, C. Hermans, and A. C. Vandaele (2002), New water vapor line parameters in the 26,000–13,000 cm^{-1} region, *J. Quant. Spectrosc. Radiat. Transfer*, *74*, 493–510.

Curcio, J. A., L. F. Drummeter, and T. H. Cosden (1955), The absorption spectrum of the atmosphere from 4400 to 5500A, *NRL Rep. 4669*, Nav. Res. Lab., Washington, D. C.

Fayt, C., and M. Van Roozendael (2001), WINDOAS user manual, Belg. Inst. for Space Aeron., Brussels.

Greenblatt, G. D., J. J. Orlando, J. B. Burkholder, and A. R. Ravishankara (1990), Absorption measurements of oxygen between 330 and 1140 nm, *J. Geophys. Res.*, *95*, 18,577–18,582.

Harder, J. W., and J. W. Brault (1997), Atmospheric measurements of water vapor in the 442-nm region, *J. Geophys. Res.*, *102*, 6245–6252.

Harder, J. W., J. W. Brault, P. V. Johnston, and G. H. Mount (1997), Temperature-dependent NO_2 cross sections at high spectral resolution, *J. Geophys. Res.*, *102*, 3861–3880.

Hermans, C., A. C. Vandaele, M. Carleer, S. Fally, R. Colin, A. Jenouvrier, B. Coquart, and M.-F. Mérienne (1999), Absorption cross-sections of atmospheric constituents: NO_2, O_2, and H_2O, *Environ. Sci. Pollut. Res.*, *6*(3), 151–158.

Hermans, C., A. C. Vandaele, S. Fally, M. Carleer, R. Colin, B. Coquart, A. Jenouvrier, and M. F. Mérienne (2002), Absorption cross-section of the collision-induced bands of oxygen from the UV to the NIR, paper presented at NATO Advanced Research Workshop, Weakly Interacting Molecular Pairs: Unconventional Absorbers of Radiation in the Atmosphere, St. Petersburg, Russia.

Hofmann, D., et al. (1995), Intercomparison of UV/visible spectrometers for measurements of stratospheric NO_2 for the Network for the Detection of Startospheric Change, *J. Geophys. Res.*, *100*, 16,765–16,791.

Kromminga, H., J. Orphal, P. Spietz, S. Voigt, and J. P. Burrows (2003), The temperature dependence (213–293 K) of the absorption cross-sections of OClO in the 340–450 nm region measured by Fourier-transform spectroscopy, *J. Photochem. Photobiol. A*, *157*, 149–160.

Kurucz, R. L., I. Furenlid, J. W. Brault, and L. Testerman (1984), Solar flux atlas from 296 nm to 1300 nm, in *National Solar Observatory Atlas*, Harvard Univ., Cambridge, Mass.

Lee, A. M., H. K. Roscoe, D. J. Oldham, J. A. Squires, A. Sarkissian, and J.-P. Pommereau (1994), Improvements to the accuracy of zenith-sky measurements of NO_2 by visible spectrometers, *J. Quant. Spectrosc. Radiat. Transfer*, *52*, 649–657.

Orphal, J. (2002), A critical review of the absorption cross-sections of O_3 and NO_2 in the 240–790 nm. Part 2. Nitrogen dioxide, *ESA-Tech. Note MO-TN-ESA-GO-0302*, Eur. Space Agency, Paris, 15 March.

Platt, U. (1994), Differential Optical Absorption Spectroscopy (DOAS), in *Air Monitoring by Spectroscopic Techniques*, edited by M. W. Sigrist, pp. 27–84, John Wiley, Hoboken, N. J.

Pommereau, J. P., and F. Goutail (1988), O_3 and NO_2 ground-based measurements by visible spectrometry during Arctic winter and spring 1988, *Geophys. Res. Lett.*, *15*, 891–894.

Preston, K. E., R. L. Jones, and H. K. Roscoe (1997), Retrieval of NO_2 vertical profiles from ground-based UV-visible measurements: Methods and validation, *J. Geophys. Res.*, *102*, 19,089–19,097.

Roscoe, H. K., D. J. Fish, and R. L. Jones (1996), Interpolation errors in UV-visible spectroscopy for stratospheric sensing: Implications for sensitivity, spectral resolution, and spectral range, *Appl. Opt.*, *35*(3), 427–432.

Roscoe, H. K., et al. (1999), Slant column measurements of O_3 and NO_2 during the NDSC intercomparison of zenith-sky UV-Visible spectrometers in June 1996, *J. Atmos. Chem.*, *32*, 281–314.

Rothman, L. S., et al. (2003), The HITRAN Molecular Spectroscopic Database: Edition of 2000 including updates through 2001, *J. Quant. Spectrosc. Radiat. Transfer*, *82*, 5–44.

Tornkvist, K. K. (2000), The development of the SYMOCS instruments and the spectral analysis, *NILU TR 1/2000*, Norw. Inst. for Air Res., Kjeller, Norway.

Tornkvist, K. K., D. W. Arlander, and B.-M. Sinnhuber (2002), Ground-based UV measurements of BrO and OClO over Ny-Alesund during winter 1996 and 1997 and Andoya during winter 1998/99, *J. Atmos. Chem.*, *43*, 75–106.

Vandaele, A. C., C. Hermans, P. C. Simon, M. Carleer, R. Colin, S. Fally, M.-F. Mérienne, A. Jenouvrier, and B. Coquart (1998), Measurements of the NO_2 absorption cross-section from 42,000 cm^{-1} to 10000 cm^{-1} (238–1000 nm) at 220 K and 294 K, *J. Quant. Spectrosc. Radiat. Transfer*, *59*, 171–184.

Vaughan, G., et al. (1997), An intercomparison of ground-based UV-visible sensors of ozone and NO_2, *J. Geophys. Res.*, *102*, 1411–1422.

Wittrock, F., H. Oetjen, A. Richter, S. Fietkau, T. Medeke, A. Rozanov, and J. P. Burrows (2004), MAX-DOAS measurements of atmospheric trace gases in Ny-Alesund—Radiative transfer studies and their application, *Atmos. Chem. Phys.*, *4*, 955–966.

G. Braathen and K. Tørnkvist, Norwegian Institute for Air Research, P.O. Box 100, 2007 Kjeller, Norway.

S. Bugarski, U. Frieß, K. Pfeilsticker, R. Sinreich, and T. Wagner, Institute of Environmental Physics, University of Heidelberg, Im Neuenheimer Feld 229, D-69120 Heidelberg, Germany.

G. Corlett and R. Leigh, Space Research Centre, University of Leicester, University Road, Leicester, LE1 7RH, UK.

C. Fayt, F. Hendrick, C. Hermans, F. Humbled, A. C. Vandaele, and M. Van Roozendael, Belgian Institute for Space Aeronomy, 3 av. Circulaire, B-1180 Brussels, Belgium. (annc@oma.be)

M. Gil, M. Navarro, O. Puentedura, and M. Yela, Instituto Nacional de Tecnica Aerospacial, Car. Ajalvir Km 4, 28850 Torrejon de Ardoz, Spain.

F. Goutail, A. Mieville, and J.-P. Pommereau, Service d'Aéronomie du CNRS, BP3, 91371 Verrières le Buisson, France.

P. Johnston and K. Kreher, National Institute of Water and Atmospheric Research, PB 50061, Omakau, Central Otago, New Zealand.

S. Khaikine, Central Aerological Observatory, 3 Pervomayskaya str., Dolgoprudny, Moscow Region, 141700, Russia.

H. Oetjen, A. Richter, and F. Wittrock, Institute of Environmental Physics, University of Bremen, Otto-Hahn-Allee, D-28359 Bremen, Germany.

K. Stebel, Polar Environmental Centre, Norwegian Institute for Air Research, 9296 Tromsø, Norway.

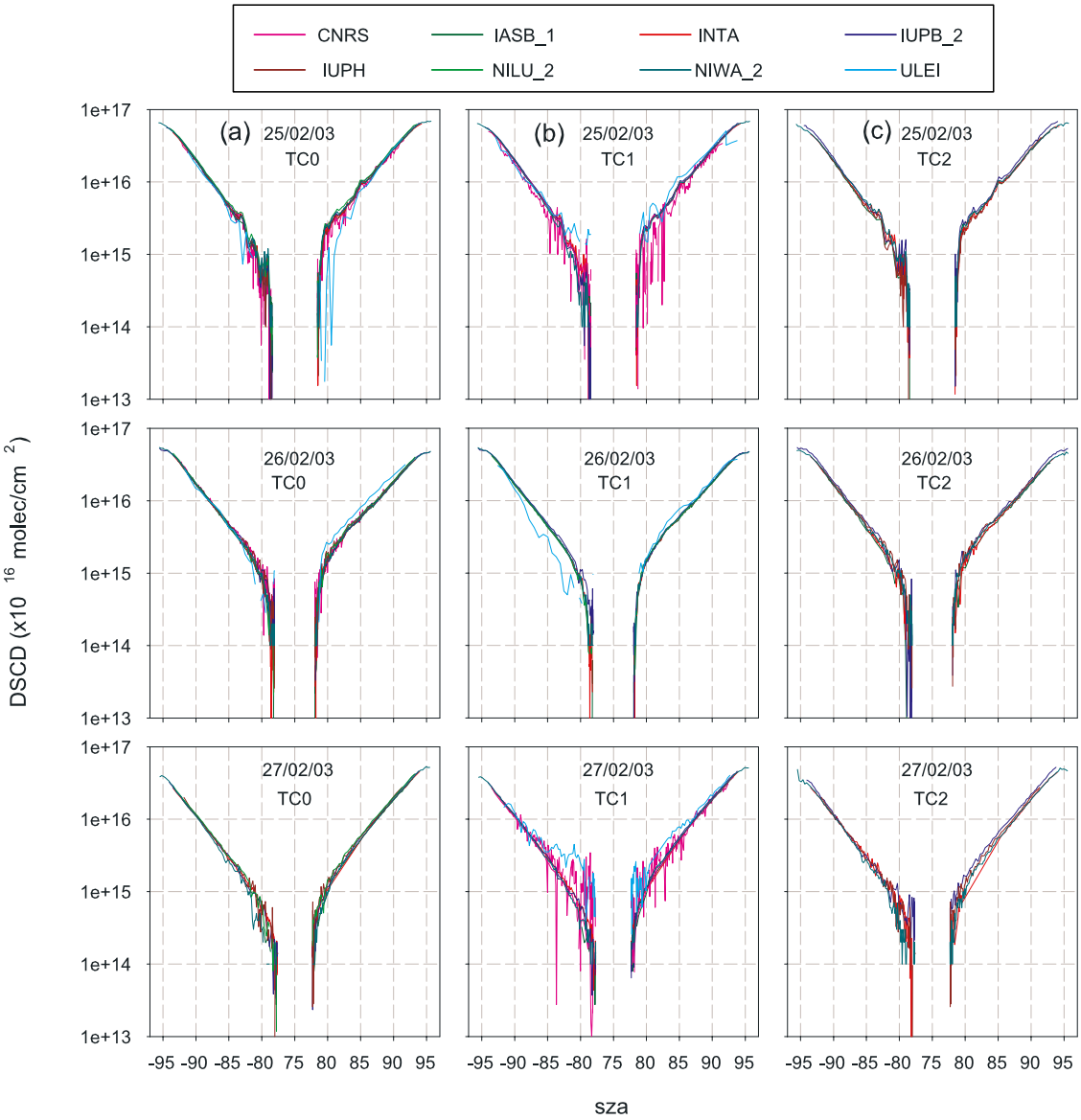

Figure 6. NO_2 DSCDs measured by all groups on February 26, 27, and 28 for (a) TC0, (b) TC1, and (c) TC2 settings. The color code is also given on the figure.

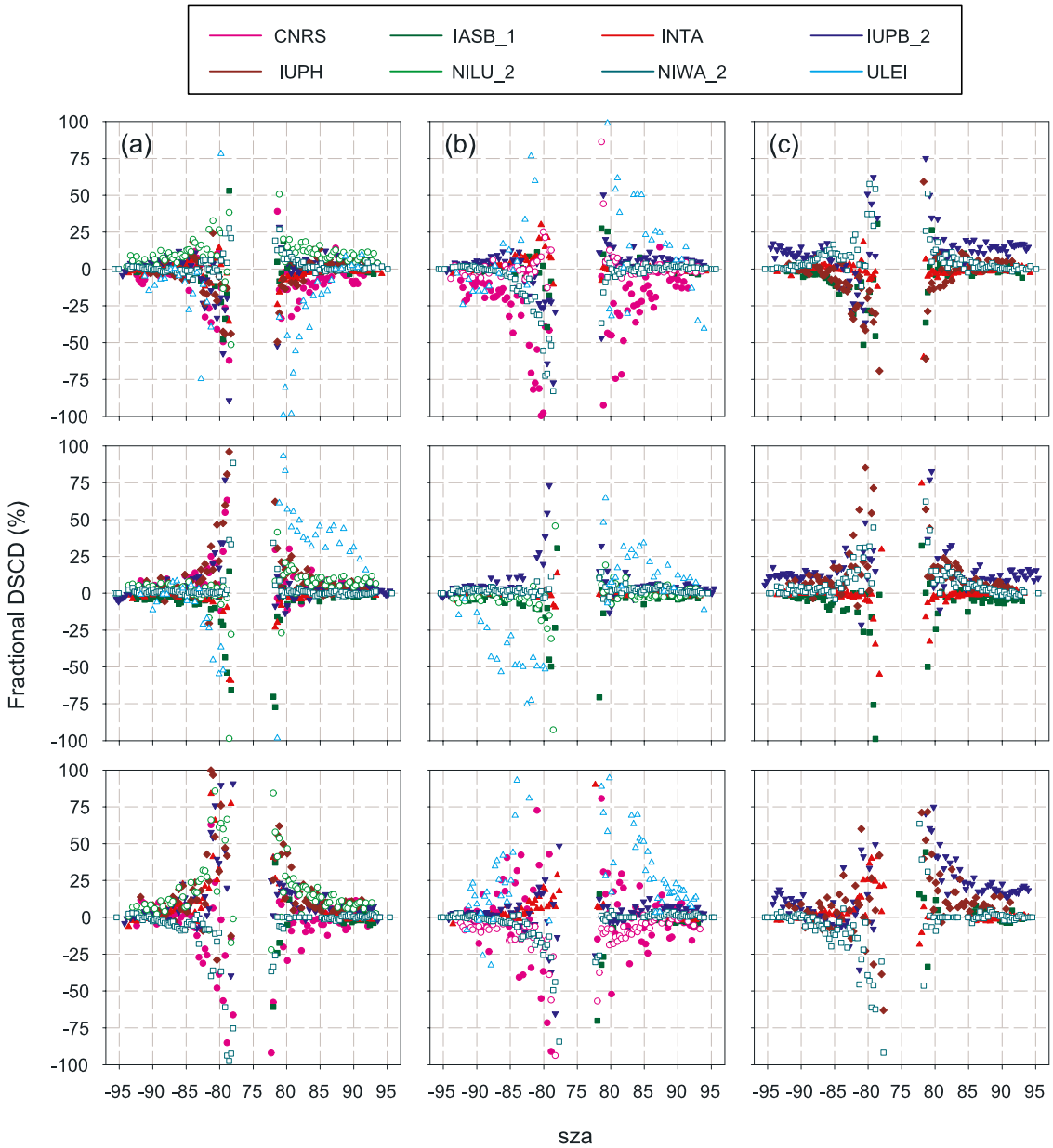

Figure 7. NO_2 fractional differences for all groups on February 26, 27, and 28 for (a) TC0, (b) TC1, and (c) TC2 settings (solid circles, CNRS; solid squares, IASB_1; solid triangles, INTA; solid inverted triangles, IUPB_2; solid diamonds, IUPH; open circles, NILU_2; open squares, NIWA_2; open triangles, ULEI).